27 September 2016

Improved retrieval of land ice topography from CryoSat-2 data and its impact for volume change estimation of the Greenland Ice Sheet

Johan Nilsson[1], Alex Gardner[1], Louise Sandberg Sørensen[2] and Rene Forsberg[2]

[1]Jet Propulsion Laboratory, California University of Technology

[2] DTU Space, National Space Institute, Technical University of Denmark

Abstract

A new methodology for retrieval of glacier and ice sheet elevations and elevation changes from CryoSat-2 data is presented. Surface elevations and elevation changes determined using this approach show significant improvements over ESA's publically available Cryosat-2 elevation product (L2 Baseline-B), compared to near-coincident airborne laser altimetry from NASA's Operation IceBridge and seasonal height amplitudes from the Ice, Cloud, and Elevation Satellite (ICESat).

Applying this methodology to CryoSat-2 data collected in Interferometric Synthetic Aperture mode over the high relief regions of the Greenland ice sheet we find an improvement in the root-mean-square-error (RMSE) of 27% and 40% compared to ESA's L2 product in the derived elevation and elevation changes, respectively. In the interior part of the ice sheet, where CryoSat-2 operates in Low Resolution Mode, we find an improvement in the RMSE of 68% and 55% in the derived elevation and elevation changes, respectively. There is also an 86% improvement in the magnitude of the seasonal amplitudes when compared to amplitudes derived from ICESat data. These results indicate that the new methodology provides improved

Johan Nilsson 9/18/2016 5:43 PM
Deleted: . This when

tracking of the snow/ice surface with lower sensitivity to changes in near-surface dielectric properties.

To demonstrate the utility of the new processing methodology we produce elevations, elevation changes and total volume changes from Cryosat-2 data for Greenland Ice Sheet during the period Jan-2011 to Jan-2015. We find that the Greenland Ice Sheet decreased in volume at rate of 289 ± 20 $km^3 a^{-1}$, with high inter-annual variability and spatial heterogeneity in rates of loss. This rate is 65 $km^3 a^{-1}$ more negative than rates determined from ESA's L2 product, highlighting the importance of Cryosat-2 processing methodologies.

Johan Nilsson 9/22/2016 11:36 AM
Deleted: 16

1 - Introduction

The European Space Agency (ESA) launched CryoSat-2 in April 2010 tasked with monitoring the changes of the Earth's land and sea ice. CryoSat-2 carries a new type of Doppler/delay radar altimeter (Raney, 1998) referred to as SIRAL (SAR Interferometric Radar Altimeter). SIRAL operates in two different modes over land ice. Over the interior part of the ice sheets it operates as a conventional pulse limited radar system, referred to as the "Low Resolution Mode" (LRM). In more complex high-sloping terrain the system uses a novel second antenna to operate in "Interferometric Synthetic Aperture Radar" (SIN) mode. These new features allow the satellite to monitor changes in complex terrain including ice caps, glaciers and the high relief marginal areas of the ice sheets. Such areas are sensitive to changes in climate and contribute greatly to current rates of sea level rise (e.g., Gardner et al. (2013) and Shepherd et al. (2012)).

Johan Nilsson 9/18/2016 5:45 PM
Deleted: ,

Ku-band radar altimeters are insensitive to cloud cover providing superior coverage to laser altimeters (e.g., ICESat) but experience significant amounts of volume scattering, which is controlled by the time-evolving dielectric properties of the near-surface snow, firn, and ice (Lacroix et al., 2008; Remy et al., 2012). These effects can have large implications for the determination of mass change over a wide range of both spatial and temporal scales. Changing snow conditions can introduce time-varying biases in the data that, in combination with the radar

Johan Nilsson 9/18/2016 5:47 PM
Deleted: the characteristics of

signals interaction with the surface, introduce large elevation biases (0.5 - 1 m) (Nilsson et al., 2015a). This, combined with other factors such as processing methodology and surface topography, makes it difficult to measure small changes for much of the word's ice covered regions (Arthern et al., 2001; Gray et al., 2015; Nilsson et al., 2015b).

The mitigation of these effects in the processing of radar altimetry data is required for improved accuracy of derived temporal and spatial changes in surface elevation of glaciers and ice sheets. Several studies have proposed different approaches to assess these effects and improve the retrieval process of surface elevation and elevation changes from radar altimetry data. These include different approaches to waveform retracking (Davis, 1993, 1997; Gray et al., 2015; Helm et al., 2014) and empirical corrections to the estimated surface elevation changes (Davis and Ferguson, 2004; Flament and Rémy, 2012; Sørensen et al., 2015; Wingham et al., 2006b; Zwally et al., 2005, 2011). Relatively little work has been done to assess methods for improving elevation and elevation changes derived from ESA's CryoSat-2 data (Abulaitijiang et al., 2015; Gray et al., 2013, 2015; Helm et al., 2014).

Here we conduct a thorough analysis of CryoSat-2 SIN and LRM waveform retracking and geolocation methodologies to design an optimal processing methodology for CryoSat-2 elevation retrieval over both smooth and complex ice-covered terrain. We then analyze several different approaches to determining surface elevation and volume changes from the scattered CryoSat-2 elevation retrievals. The overarching goal of this work is to develop robust and accurate elevation retrieval algorithms that are less sensitive to changes in surface and sub-surface scattering properties.

The new processing scheme is applied to estimate elevation and volume changes of the Greenland Ice Sheet for the period January 2011 to January 2015, using two independent methods to characterize the robustness of the results due to methodology. The results are compared to change estimates obtained from the ESA L2 Baseline-B surface elevation product (Bouzniac et al., 2014), high accuracy airborne data from NASA IceBridge airborne topographic

Johan Nilsson 9/18/2016 5:50 PM
Deleted: from

Johan Nilsson 9/26/2016 10:22 AM
Deleted: t

Johan Nilsson 9/26/2016 10:22 AM
Deleted: hat

mapper and seasonal height amplitudes estimated from Ice, Cloud, and Elevation Satellite (ICESat) data.

2 - Surface elevations from CryoSat-2

Johan Nilsson 9/26/2016 10:23 AM
Deleted:

2.1 - Low Resolution Mode (LRM)

The LRM mode is used over the interior parts of the ice sheet, which mostly consist of low sloping terrain. Here, SIRAL operates as a conventional pulse limited radar system with a transmission frequency of 13.6 GHz (Ku-band) and has Pulse-Limited Footprint (PLF) radius of approximately 1.5 km and a beam-limited footprint (BLF) radius of approximately 7.5 km over flat terrain (Bouzinac, 2014). The gentle terrain allows for accurate mapping of the surface elevation of the ice sheet down to decimeter-level (Brenner et al., 2007). Within the LRM waveform we define the location of the surface from the leading edge of the waveform, based on a fraction of the maximum amplitude of the received power. This approach is commonly referred to as a threshold retracker. Following Davis et al. (1997) we use 20% threshold to define the location of the surface. Davis et al. (1997) argued that a 20% threshold represents the best compromise between waveforms that are entirely dominated by either volume or surface scattering, making it suitable for obtaining estimates of surface elevation for most parts of the Greenland Ice Sheet.

Johan Nilsson 9/18/2016 5:56 PM
Deleted: (0-1°)

The CryoSat-2 LRM radar waveforms suffer from measurement noise, in the form of speckle noise. Furthermore, over the steeper parts of the LRM-area the range gate tracking-loop can loose track of the surface, producing non-usable waveforms. To remove bad or loss of track waveforms the radar waveform (20 Hz) is first filtered using a zero-phase low pass filter to reduce speckle noise on a line-by-line basis. The signal-to-noise-ratio (SNR) of the waveform is then estimated and if the SNR < 0.5 dB the waveform is rejected. The SNR threshold was

empirically chosen to obtain a good trade-off between the quality of the measurements and sampling.

Before the waveform can be retracked the first surface return (first major peak) is identified within the range gate window. A copy of the waveform is heavily smoothed to remove small-scale surface roughness signals, keeping the overall surface signal intact. The range gate index of the first peak from the copy is then used to extract the leading edge of the original low pass filtered waveform. Only leading edges with a peak index above 20 are used in the retracking, as peaks before or after that indicate troublesome surface ranging. The extracted leading edge is then oversampled by a factor of 100 (c.f. (Gray et al., 2013; Helm et al., 2014), and the range R between the surface and satellite is determined based on the 20% threshold computed according to Davis et al. (1997). The range is then corrected for several atmospheric and geophysical effects relevant to land ice studies according to Bouzinac (2014). The surface elevation H of the topography, relative to the WGS84 ellipsoid, is estimated as $H = A - R$, where A is the altitude of the satellite.

Johan Nilsson 9/18/2016 6:01 PM
Deleted: within the interval of 20-350

The measured surface return over a sloping surface does not originate from the satellites nadir location, but from the “Point Of Closest Approach” (POCA) to the spacecraft (Brenner et al., 1983). These off-nadir returns can introduce a large range bias to the surface, depending on the magnitude of surface slope, ranging from 0-120 m (Brenner et al., 1983) as the measured surface height is mapped to an erroneous position (i.e. the nadir position). To mitigate the effect of this error we correct the measured range and location to the POCA point using an a-prior DEM, following the approach of Bamber (1994). In contrast to previous studies we account also for the local surface curvature, as Remy et al. (1989) showed that accounting for surface curvature in addition to surface slope significantly improve results. The surface slope, aspect and curvature are estimated from an a priori DEM. The GIMP elevation model (Howat et al., 2014) was used to derive surface parameters for the slope-induced error correction in the LRM mode. The DEM was resampled to 2 km resolution, using bilinear

interpolation, prior to parameter estimation, corresponding to the pulse-limited footprint of the LRM mode.

2.2 - Interferometric Synthetic Aperture Radar Mode (SIN)

The SIN mode is used over the marginal areas of the ice sheets and other smaller glaciated areas. In these areas the SIRAL altimeter operates as a Doppler/Delay radar system (Raney, 1998). The Doppler/Delay radar allows for higher along-track resolution compared to conventional altimetry, resulting in 350 m resolution in along track and 1500 m across track. In ordinary SAR operation only the amplitude of the radar echo is measured and the phase content is discarded or ignored. With the inclusion of a second antenna on CryoSat-2, interferometric SAR can also be performed. Difference in the path length between the POCA and the individual antennas introduce a phase shift between the two retrieved signals that can be related to the angle of arrival (look angle). The look angle can in turn be used to resolve the across track (across antenna) location of the echo.

Multi-look processing is applied to ESA's L1B waveform product (Bouzinac, 2014) to reduce the noise in the SIN waveform but it is still affected by speckle-noise, as is the case for the LRM waveforms. To mitigate this effect, and to help identify the leading edge of the first return, we apply speckle reduction filtering and leading edge extraction of the SIN waveforms in the same way as for the LRM processing with minor changes due to differences in range gate resolution. In this case, compared to the LRM retracking algorithm, only leading edges with a peak index in the range of 20-350 are used for retracking the radar waveform.

The estimated coherence *C* of the multi-looked waveforms is then filtered in two stages; (i) all coherence measures larger than one is set to zeros (larger than one coherence exists in the L1B product reason unknown). (ii) The coherence array, as a function of range, is filtered using a 2D 5x5 Wiener filter to remove high frequency noise. The filtering of the waveform and

Johan Nilsson 9/25/2016 5:29 PM
Deleted: .

Johan Nilsson 9/18/2016 6:10 PM
Deleted: Keith

Johan Nilsson 9/18/2016 6:17 PM
Deleted: . SIN modes allows for a

Johan Nilsson 9/18/2016 6:27 PM
Deleted: the

Johan Nilsson 9/18/2016 6:26 PM
Deleted: range power image

the coherence is applied to remove noise in the recreation of the interferogram. This is further discussed later.

The measured differential phase ϕ of the return signal is affected by phase ambiguities; a sudden shift of 2π in the measured phase. To reduce phase noise and aid the phase, an unwrapping of the radar interferogram *I* is performed according to Gray et al. (2013):

$$I = P \cdot C \cdot e^{-i\phi} \quad (1)$$

The interferogram is then filtered using a wavelet-based de-noising technique, where the real and imaginary parts of the interferogram are filtered separately. The unwrapping of the interferogram allows for indirect filtering of the phase, without being affected by the phase-ambiguities. Phase filtering is an important consideration as it has a direct affect on accuracy of the position of the ground echo. We selected a bi-orthogonal as the mother wavelet to produce the wavelet coefficients decomposed into three levels. Soft thresholding was applied to detail coefficients, using a heuristic threshold rule to remove noise at every level. This was done on a line-by-line basis. The final filtered differential phase was then recovered by:

$$\phi_f = Re\{I_f\} + Im\{I_f\} \quad (2)$$

To resolve the phase ambiguities the filtered phase measurements require unwrapping. The phase unwrapping is done on a line-by-line basis in two directions starting from the center of gravity of the waveform (Wingham et al., 1986).

The return power distribution of a Doppler/Delay radar system shows an important distinction from those from conventional pulse-limited radar systems. Here, the point corresponding to the mean surface is not located at the half-power point on the leading edge, but rather closer to the maximum (Wingham et al., 2006a). Therefore a new retracker has been developed, closely related to the one used in Gray et al. (2013), to allow for adaptive retracking of the upper parts of the leading edge of the SAR waveform. The algorithm follows the main concept of the threshold retracker, developed by Davis, (1997), but instead of a pre-defined

Johan Nilsson 9/27/2016 12:17 PM
Deleted: (

threshold it tracks the maximum gradient of the leading edge of the waveform. We refer to this approach as that “Leading-edge Maximum Gradient retracker” (LMG).

The surface returns are geolocated using the across track look-angle θ estimated from the differential phase at the retrackig point according to (Wingham et al., 2006a). This, in combination with the viewing geometry, is used to define the location of the surface return on the ground using basic across track interferometric principles. We correct θ for the interferometer surface slope error by applying the look-angle scaling factor estimated in (Galin et al., 2013).

The along-track differential phase estimate, interpolated to the retracking point, is affected by phase ambiguities not corrected for during the phase unwrapping procedure. To reduce residual phase ambiguities an a priori DEM (GIMP) is used to extract the DEM surface, resampled to 500 m resolution (corresponding to the along-track sampling), elevations at the nadir and echolocation using bilinear interpolation. Over a sloping surface the surface return should always come from a position upslope from the nadir point. Therefore the following relation must hold where ($H_{echo} > H_{nadir}$) or for a more practical application ($H_{echo} - H_{nadir}) > \varepsilon$, where ε is the uncertainty of the DEM used. If this relation is violated 2π is added or subtracted to the individual along-track phase estimate, depending on the sign.

A final step is applied to correct for any lingering phase ambiguities not corrected by the a priori DEM. This step uses the assumption that the along-track phase should follow a consistent pattern over most part of the satellite ground track. Hence, any large discrepancies from the overall pattern of the along-track phase would indicate an ambiguity. The ambiguity is detected by computing the residuals of the along-track phase by removing a smoothed version. If any of the residuals have a magnitude larger than π it is considered ambiguous and thus corrected by adding or subtracting 2π.

3 - Surface elevation changes from CryoSat-2

3.1 – Surface fit method

The surface-fitting method is based on fitting a linear model to the elevations as a function of time and space inside a search radius of 1 km (e.g., Howat et al., 2008; Moholdt et al., 2010; Sørensen et al., 2011; Wouters et al., 2015). The linear model consists of a time-invariant (static) bi-quadratic surface model to account for variable topography inside the search radius and time-variant part used to extract the temporal change in elevation. The model consists of a total of 7-parameter whereof six of the parameters (a-coefficients) describe the bi-quadratic surface modeling function, *dh/dt* the linear elevation change rate, *t* time in decimal years, t_0 the mean time inside the footprint and ε the residuals from the linear regression.

$$h(x,y,t) = a_0 + a_1 x + a_2 y + a_3 xy + a_4 x^2 + a_5 y^2 + \frac{\partial h}{\partial t}(t - t_0) + \varepsilon \quad (3)$$

The algorithm estimates the elevation change at every echolocation (or grid-node if desired) in the data set. In each solution the signal amplitude and phase are also estimated by fitting a seasonal signal model to the surface-fit elevation residuals, according to:

$$\Delta h(t) = s_0 \cos(wt) + s_1 \sin(wt) + \varepsilon \quad (4)$$

where Δh is the elevation residuals estimated from the plan-fit model, $s_{0,1}$ are the model coefficients and t the time. The amplitude *A* is then defined as $A = \sqrt{s_0^2 + s_1^2}$ and the phase *P* as $P = \tan^{-1}\left(\frac{s_1}{s_0}\right)$.

To remove outliers an iterative 3σ-filter is used in the full model solution, i.e. the topography, trend and seasonal signal are removed, using a maximum of 5-iterations. For each iteration residuals (full-model) with an absolute value larger than 10 m are removed, as seasonal changes larger than 10 m are not expected (Moholdt et al., 2010; Wenlu Qi and Braun, 2013). The data inside the 1 km cap is weighted according to their distance from the estimation point according to:

Johan Nilsson 9/19/2016 11:23 AM
Deleted: 0-5

Johan Nilsson 9/19/2016 11:27 AM
Formatted: Font:Italic

Johan Nilsson 9/19/2016 11:27 AM
Formatted: Font:Italic

Johan Nilsson 9/19/2016 11:27 AM
Formatted: Font:Italic

Johan Nilsson 9/19/2016 11:27 AM
Formatted: Font:Italic, Subscript

Johan Nilsson 9/19/2016 11:27 AM
Formatted: Font:Italic

Johan Nilsson 9/19/2016 11:24 AM
Deleted: .

Johan Nilsson 9/19/2016 11:21 AM
Deleted: H

Johan Nilsson 9/19/2016 11:22 AM

Johan Nilsson 9/19/2016 11:20 AM
Deleted: a_6

Johan Nilsson 9/19/2016 11:20 AM
Deleted: dt

Johan Nilsson 9/19/2016 11:21 AM
Deleted: H

Johan Nilsson 9/19/2016 11:10 AM
Deleted: 7

Johan Nilsson 9/19/2016 11:11 AM
Deleted: a

Johan Nilsson 9/19/2016 11:11 AM
Deleted: 8

Johan Nilsson 9/19/2016 11:27 AM
Deleted: *H*

Johan Nilsson 9/19/2016 11:27 AM
Deleted: *a*

Johan Nilsson 9/19/2016 11:11 AM
Deleted: a

$$W = \frac{1}{\left(1+\left[\frac{d}{\rho}\right]^2\right)} \quad (5)$$

where W is the estimated weight, d the distance and ρ the correlation or resolution parameter set to 500 m. The weighting allows the solution to better reflect local signal dynamics at the prediction point.

Local elevation time-series are further computed from the elevation residuals and elevation trend from each solution, according to:

$$h(x, y, t) = (t - t_0) \cdot \frac{\partial h}{\partial t} + \varepsilon \quad (6)$$

where t is the time epochs inside the search cap, t_0 is the mean time of t, dh/dt is the elevation change rate and $\varepsilon(t)$ is the elevation residual at each time epoch.

The elevation changes estimated from the surface-fitting method are then culled to remove outliers before spatial gridding. Elevation changes with a regression error larger than 15 m a^{-1} are removed. The resulting surface elevations are binned at 5-km resolution for outlier editing purposes. For each cell the local spatial trend is modeled as a bilinear surface, and removed. The residuals are then edited using an iterative 3σ filter until the RMS converges to 2%.

3.2 – Crossover method

The crossover method is used to derive surface elevation at the intersection point between an ascending and descending satellite ground track separated in time (Brenner et al., 2007; Khvorostovsky, 2012; Zwally et al., 1989). The surface elevations and times are then estimated at the crossover location for each track by linear interpolation of the two closest data points. The crossover height difference is then estimated by taking the height difference between the two tracks according to:

$$\Delta h = h_2 - h_1 + \varepsilon \quad (7)$$

were h_1 and h_2 are the surface heights at the crossover location at time epoch t_1 and t_2, respectively, and E is the random measurement error, including orbital, range and retracking errors.

This approach produces crossover height differences with scattered time-epochs ranging from 0-4 years. CryoSat-2 has a 369-day repeat orbit configuration with a 30-day sub-cycle meaning that each crossover location will be revisited every 369 days and surrounding area every 30 days. This produces annual and sub-annual crossover difference around each crossover location. This fact is used to produce elevation change rates by incorporating all multi-temporal crossover difference within a neighborhood of 2.5-km around each crossover location. The elevation change is then estimated using the same procedure described for the surface-fit method, except that a bilinear model is used to remove any spatial trends in the topography of the crossover elevations according to:

$$dh(x, y, t) = a_1 x + a_2 y + \frac{\partial h}{\partial t}(t - t_0) \quad (8)$$

where dh is the crossover height difference, $(t-t_0)$ the time difference, a_1 and a_2 the across and along-track slope and dh/dt the elevation change rate. This produces elevation changes comparable in time and in spatial coverage with the surface-fit method. The same outlier editing schemes is applied to the crossover elevation change rates as for the surface-fit method.

3.3 - Gridding of sparse elevation and elevation change data

The gridding is done in a polar-stereographic projection with a latitude of origin at 70°N, central longitude of 45°W and origin at the North Pole. The projection is referenced against the WGS-84 ellipsoid and the grid-resolution. The observations derived from the surface-fit are gridded at a resolution of 1x1-km, due to the high spatial sampling.

The method of Least Squares Collocation (LSC), described in Herzfeld (1992) is used to grid the observations onto a regular grid. LSC is similar to Kriging and allows for optimal

(9)

Johan Nilsson 9/19/2016 11:35 AM
Deleted: H

Johan Nilsson 9/19/2016 11:34 AM
Deleted: 0

Johan Nilsson 9/19/2016 11:34 AM
Deleted: 1

Johan Nilsson 9/19/2016 11:34 AM
Deleted: $a_2 dt$

Johan Nilsson 9/19/2016 11:36 AM
Deleted: d

Johan Nilsson 9/19/2016 11:36 AM
Deleted: H

Johan Nilsson 9/19/2016 11:35 AM
Deleted: d

Johan Nilsson 9/19/2016 11:36 AM
Deleted: $_0$

Johan Nilsson 9/19/2016 11:36 AM
Deleted: $_1$

Johan Nilsson 9/19/2016 11:36 AM
Formatted: Font:Italic

Johan Nilsson 9/19/2016 11:36 AM
Formatted: Font:Italic

Johan Nilsson 9/19/2016 11:36 AM
Formatted: Subscript

Johan Nilsson 9/19/2016 11:36 AM
Formatted: Font:Italic

Johan Nilsson 9/19/2016 11:36 AM
Formatted: Not Superscript/ Subscript

Johan Nilsson 9/19/2016 11:36 AM
Deleted: a_2

Johan Nilsson 9/20/2016 10:02 AM
Deleted: 3.3 – DEM method . ... [1]

Johan Nilsson 9/20/2016 10:02 AM
Deleted: 4

interpolation and merging of data with different accuracies, using their inherent covariance structure. The LSC-algorithm uses the 25 closest data points in 8-quadrants surrounding the prediction point to reduce spatial biasing. The prediction equation consists of two terms where the first term is the actual prediction term and the second term accounts for the non-stationary part of the data, as described by:

$$\hat{s} = C_{sz}(C_{zz} + N)^{-1} z + \left(1 - \sum (C_{sz}(C_{zz} + N)^{-1})\right) m(z)$$

were C_{sz} is the cross-covariance, C_{zz} is the auto-covariance, N the diagonal noise-matrix consisting of the a priori RMS-error and $m(z)$ is the median value of the observations inside the search neighborhood.

The covariance of the data inside the local neighborhood is modeled as a function of distance away from the prediction point using a third-order Gauss-Markov model described below.

$$C(r) = C_0 \left(1 + \frac{r}{\alpha} - \frac{r^2}{2\alpha^2}\right) e^{\left(-\frac{r}{\alpha}\right)} \quad (10)$$

where r is the separation distance, C_0 the local data variance and α is a scaling factor estimated from the correlation length.

LSC interpolation provides a RMS-error for each prediction point estimated from the modeled covariance of the data according to:

$$C_{\hat{s}} = C_0 - C_{sz}(C_{zz} + N)^{-1} C_{sz}^T \quad (11)$$

where the RMSE of the prediction equals to $\sigma_{\hat{s}} = (C_{\hat{s}})^{1/2}$ and where C_{sz}^T is the transposed cross-covariance matrix.

The elevation changes estimated from the surface-fit and crossover methods are interpolated to a regular grid using their a priori error estimated from the LSC scheme. To avoid unrealistically small errors, common in the regression errors estimated over flat terrain, a minimum error threshold is applied. Error values smaller than a specific threshold are set to the threshold value. The threshold value is representative of the overall precision of the elevation

Johan Nilsson 9/19/2016 11:37 AM
Deleted: y

Johan Nilsson 9/19/2016 11:46 AM
Deleted: xy

Johan Nilsson 9/19/2016 11:47 AM
Deleted: xx

Johan Nilsson 9/19/2016 11:47 AM
Deleted: x

Johan Nilsson 9/19/2016 11:47 AM
Deleted: xy

Johan Nilsson 9/19/2016 11:47 AM
Deleted: xx

Johan Nilsson 9/19/2016 11:47 AM
Deleted: x

Johan Nilsson 9/19/2016 11:47 AM
Deleted: xy

Johan Nilsson 9/19/2016 11:47 AM
Deleted: xx

Johan Nilsson 9/19/2016 11:48 AM
Deleted: x

Johan Nilsson 9/19/2016 11:48 AM
Deleted: data

Johan Nilsson 9/19/2016 11:49 AM
Deleted: y

Johan Nilsson 9/19/2016 11:49 AM
Deleted: y

Johan Nilsson 9/19/2016 11:49 AM
Deleted: xy

changes over flat terrain and is set to 0.2 m a^{-1}. The data are then gridded using a 75 km correlation length determined from the comparison of CryoSat-2 elevation to airborne measurements (Section 5).

Johan Nilsson 9/21/2016 6:14 PM
Deleted: 50

The LSC algorithm is also used to generate a DEM based on the surface elevations generated from the surface-fitting algorithm. The surface elevations generated from the surface-fit were used as input to the gridding-algorithm. The use of surface elevations from the surface-fit provides several advantages compared to the raw observations as they: provide an almost equal number of observations as the raw data, have been screened for gross outliers, have been low-pass filtered using the 1-km search radius, and are all reference to the same time epoch. Further the RMSE error generated from the surface-fit estimated surface height can be used as an a priori error for the LSC gridding procedure.

The DEM is generated using the same approach as for the surface elevation changes, as described previously in the section. Before the gridding procedure is applied elevations $H < 0$ and $H > 3350$ m are removed from the data set. Further, elevations with a standard error larger than 30 m are also removed. The elevations are binned spatially into a resolution of 1000 m and inside each cell the local surface trend is removed by fitting of a planar surface, and an iterative 3σ filter is applied to the residuals to remove outliers.

4 - Surface elevations and elevation changes from ICESat

To assess basin-scale patterns of elevation change we compare elevation changes from CryoSat-2 data to elevation changes derived from Ice, Cloud, and Elevation Satellite (ICESat) data. Here we use release 33 (GLA06) data collected over the 2003-2009 period. The ICESat surface heights were used to generate surface elevation changes and seasonal parameters according to method M3 in Sørensen et al. (2011). The derived elevation changes were corrected for the G-C offset (Borsa et al., 2014). Valid elevation retrievals were selected

according to Nilsson et al. (2015b). The ICESat elevation, seasonal amplitude and phase, are then used for comparison with CryoSat-2 and to build continuous time series using the surface fit method described in Section 3.1. For the purpose of this study no correction for the inter-campaign bias was applied, as this is still an active area of investigation.

5 -Validation

Elevation and elevation change results were generated for the entire Greenland Ice Sheet using CryoSat-2 data collected between Jan-2011 and Jan-2015 using the methodology presented in (Sections 2-3) (JPL product) and by applying the methods of (Section 3) to ESA's CryoSat-2 L2 elevation products (ESA product). Surface elevations and elevation changes were validated against airborne data sets obtained from NASA's Operation Ice-Bridge Airborne Topographic Mapper (ATM), obtained from the "National Snow & Ice Data Center" (NSIDC) in the form of the ILATM2 product. The generated elevation product has a resolution of 80 m, with a 40 m spacing along-track. This mission produces both elevation and elevation changes with reported vertical accuracy of ~10 cm and temporal accuracy in the cm-level (Krabill et al., 2002).

The derived surface elevations from CryoSat-2 are differenced against ATM surface elevations within 50 m of each ATM locations. One month of CryoSat-2 data consistent in time with the ATM elevations are used for the validation to avoid biases due to temporal sampling and to obtain sufficient sample size. A total of four years of campaign data are used for the validation of the surface elevations (2011-2014). The residuals are edited using an iterative 3σ filter to remove outliers. The accuracy and precision is estimated as the mean and standard deviation of the differences, respectively. The residual distribution is further binned according to surface slope estimated from the GIMP DEM (Howat et al., 2014) resampled to 500 m. The sensitivity to surface slope (slope error) can be identified in the standard deviation of the binned residuals and can be used to judge the quality of the produced surface elevation and elevation

Johan Nilsson 9/20/2016 10:03 AM
Deleted:

Johan Nilsson 9/19/2016 1:06 PM
Deleted:

Johan Nilsson 9/22/2016 3:50 PM
Deleted: (slope error) is then defined by fitting a 1st order polynomial to the slope and height residuals. The rate estimated from the polynomial provides an indication of the magnitude of the slope-induced error over the entire slope interval.

changes, while the binned-average for the elevations can be used to determine radar-signal penetration.

Surface elevation change rates estimated from three different time-periods (2012-2014, 2011-2013 and 2011-2014) of overlapping ATM observations (Krabill, 2014) are used to validate the surface elevation changes estimated from the CryoSat-2 data. The same validation methodology applied to surface elevations is applied to surface elevation changes, with a few minor modifications. First the search radius is increased to 175 m to make it conform to the ATM elevation change resolution of 250 m, as this search radius encloses the entire ATM grid cell. Secondly the estimated mean and standard deviation are multiplied with the individual time-intervals of the validation data sets to make the errors comparable.

For the surface-fit and crossover methods, near-coincident elevation change rates were compared with ATM rates (e.g., April-2011 to April-2014). This provided three validation data sets for the surface-fit method, due to its high spatial coverage. However, only the 2011-2014-validation data set could be used for the crossover method, due to the lower spatial sampling of the crossovers.

The overall accuracy and precision for both the surface elevation and elevations changes are then estimated by taking the weighted mean, using the number of observations as weights, for each data set giving an average error for each measurement mode, as seen in Table-2. The weighted average errors for each mode and method have been summarized in Table-1 and Table-2 for both the ESA's and our solutions, where the values for the individual campaigns can be found in the Supplementary material.

The estimated surface elevation changes from the two independent methods were validated separately using near-coincident ATM data. In general we find the same magnitude of improvement observed in the surface elevation validation analysis. The statistics of the elevation change validation have been summarized in Table-2 for each method independently for the two modes of instrument operation. We find the lowest RMSE errors for the surface-fit

Johan Nilsson 9/20/2016 10:04 AM
Deleted: The observational error for the DEM-method is estimated similarly as for the surface-fit method, with some modifications. Here, the CryoSat-2 DEM is used to de-trend the corresponding months of CryoSat-2 data consistent with the months used to derive the ATM-elevation changes (e.g., April 2011 to April-2014). However, the monthly spatial CryoSat-2 coverage does not provide adequate number of comparison points. Thus the months of March and May were included in the analysis (i.e. March-May 2011 to March-May 2014) to increase the number of samples.

Johan Nilsson 9/22/2016 11:15 AM
Deleted: three

method, followed by the crossover method. This differs from the findings of Moholdt et al. (2010) who found lower intrinsic errors for the crossover method, compared to the surface-fit method when applied to ICESat data. The larger search radius used for our application of the crossover method most likely explains the difference in findings between studies. Further, we find that the surface-fit method provides the largest reduction in RMSE for the JPL product, corresponding to 40% and 55% for the SIN and LRM-mode, respectively.

The correlation length used to derive the number of un-correlated grid-cells, which is used to estimate the standard error, was determined from a semi-variogram analysis of the elevation change residuals from CryoSat-2 minus ATM using the data from the surface-fit method. The comparison was done for each mode separately for all the individual campaigns and multiplied with the their individual time span. The semi-variogram was then computed from all the time-invariant residuals, to maximize the spatial coverage, for each mode. Analysis of the semi-variogram showed an approximate correlation lengths of 100 and 75 km for the SIN and LRM-mode respectively. These correlation lengths are inside the range of the ones found by Sørensen et al. (2011) for their analysis of ICESat data, which was found to be 50-150 km.

Although the main goal of this study is not to derive or compare different types of DEM's they do play a critical part in removing the long-wavelength topography in order to derive the monthly time-series of volume change from the DEM-method. To gain insight into the overall quality of our CryoSat-2 derived DEM (referred to as JPL) we compare it to three other DEM's derived from other data sets. Firstly, we compare it to a DEM derived from ESA CryoSat-2 L2 data (referred to as ESA) gridded in the same manner as our DEM (Section 3.3). Secondly we compare it to a DEM from Helm et al. (2014), also based on CryoSat-2 data from 2011-2014 (referred to as AWI). Thirdly, we compare to a DEM from Howat et al. (2014) (which was used to derive topographical parameters and corrections for the JPL CryoSat-2 data), based on photogrammetry data from 1999-2002 co-registered to ICESat elevation data from 2003-2009 (referred to as GIMP).

Johan Nilsson 9/20/2016 10:04 AM
Deleted: and then the DEM method

Johan Nilsson 9/21/2016 6:03 PM
Deleted: 25

Johan Nilsson 9/21/2016 6:03 PM
Deleted: 35

Johan Nilsson 9/21/2016 6:07 PM
Deleted: ese

Johan Nilsson 9/21/2016 6:06 PM
Deleted: slightly lower than

Johan Nilsson 9/21/2016 6:08 PM
Deleted: ose

Johan Nilsson 9/21/2016 6:07 PM
Deleted: . To be conservative we chose a correlation length of 50 km for both modes.

Johan Nilsson 9/21/2016 6:07 PM
Deleted: .

Johan Nilsson 9/20/2016 10:05 AM
Comment [1]:

Johan Nilsson 9/20/2016 10:05 AM
Deleted: 4

Johan Nilsson 9/22/2016 4:02 PM
Deleted: .

These data sets were then compared to IceBridge ATM elevations, spanning the four different campaigns previously used for validation of the CryoSat-2 elevations. The DEM elevation was estimated at each ATM location, using bilinear interpolation, and the elevation difference computed as (DEM-ATM). No attempt was made to account for differences in DEM and ATM epochs. The estimation of the errors of the DEM was determined in the same way as for the individual CryoSat-2 surface heights. The results of the comparison have been summarized in Table-3, as the weighted average of the different campaigns. The values from each individual campaign can be found in the supplementary material.

Analyzing the overall RMSE we find that the AWI produces the lowest RMSE, followed by JPL, ESA and GIMP, due to AWI's lower standard deviation. However, the best accuracy is obtained by the JPL DEM, which shows the lowest elevation bias of all DEM's. The ESA derived DEM shows a slightly better standard deviation than the JPL DEM, which can be explained by higher data density in the marginal areas for the ESA data. The difference in density is due to the SNR rejection criterion applied in our elevation processing. This smoothing can explain the lower standard deviations seen for the AWI product. The GIMP data set showed higher degrees of impulse noise than the other products, explaining the higher observed standard deviation. This impulse noise is attributed to that local elevation change rate, which was not accounted for in the creation of the DEM (Howat et al., 2014). Overall we find that the JPL DEM provides a suitable compromise between resolving of local detail and the minimization of bias. Further, modification to the SNR filtering criteria will likely lead to additional improvements in the DEM.

To determine the effect of retracking on the accuracy and precision of the measured surface heights from CryoSat-2 several tests was performed over different parts of Greenland for both modes. Following the approach of Davis (1997) the accuracy (mean) and precision (standard deviation) was computed as a function of leading edge threshold (in percent). This computation was performed using a standard leading-edge threshold retracker, referred from now on as LTH, for both the LRM and SIN mode independently. The validation was performed

Johan Nilsson 9/23/2016 3:19 PM
Formatted: Indent: First line: 0.5"

in the same manner as described in Section 5, where ATM elevations from 2013 was used as the surface reference.

For the LRM mode data from April 2013 from the northern parts of Greenland, spanning the region 75-81°N and 54-44°W, was used to calculate height residuals for the different thresholds. This produced approximately 1000 comparison locations, which was used to calculate statistics. The same procedure was performed over Jakobshavn Isbræ, using the same time span, to calculate statistics for the SIN-mode providing roughly 2500 comparison locations.

The results of this analysis, summarized in Figure-2, show that for the LRM-mode that the precision (as a function of threshold) follows the same behavior as observed by Davis (1997), with a decrease of precision following increasing retracking threshold. However, the most notable finding was the observed inverse relationship in precision for the SIN-mode compared to LRM. For LTH-algorithm, in the SIN-mode, we observe a clear increase in precision as the retracking threshold increases, seen in Figure-2, stabilizing around 30-40%. Analyzing the accuracy derived from the different thresholds a clear difference in apparent penetration depth of the radar signal can be observed for the two modes. For the SIN-mode, below 40%, a positive bias is observed indicating that retracker produces elevations larger than the corresponding airborne measured heights. For thresholds larger than 40% surface penetration of the signal is observed which are in general closer to the surface compared to the LRM-mode. We attribute this to differences in the near-surface density structure covered by the two modes.

In general we conclude that for the LRM-mode that low retracking thresholds (0-30%) reduces the magnitude of the apparent surface penetration bias and provides higher precision compared to higher thresholds. Therefore, a threshold of ~20% of the leading edge is suggested for retracking surface elevations for the LRM-mode, which was also previously suggested by Davis (1997) and Helm et al. (2014). However, for the SIN mode a threshold

Johan Nilsson 9/23/2016 3:20 PM
Formatted: Indent: First line: 0.5"

below 40% is not recommended, as this produces a clear positive elevation bias and poor precision, as seen in Figure-2. Analyzing the difference between the LTH and the adaptive LMG algorithm, used in the SIN-mode, we find that the LMG algorithm produces superior results in precision compared to the standard LTH-algorithm. Comparing the adaptive solution from LMG to the optimum threshold found by the LTH-algorithm, we find a comparable magnitude of the elevation bias and a 32% improvement in precision, with an overall 27% reduction in RMSE, using the LMG-retracker. Studying the results from this comparison between the two-retracker algorithms we recommend the use of the adaptive threshold approach, as it produces an elevation repeatability that exceeds that of the standard threshold retracker and provides a low penetration bias.

A case study was also performed to determine the different processing steps affect on the quality of the retrieved observations. For this purpose the Barnes ice cap, on Baffin Island in the Canadian Arctic, was chosen due to its small size, excellent validation coverage and due to that it consist mostly of super-imposed ice (reducing radar signal penetration). The ice cap saw a major IceBridge ATM campaign in 2011 providing a large number of flight tracks (spanning in both North-South and East-West directions) suitable for validating CryoSat-2 data. The result of this case study, which is detailed in supplementary material (i.e. Table-S1) shows that the filtering of the differential phase has the highest impact on the overall accuracy of the observation, reducing the RMSE with 12%, followed by the ambiguity correction. This shows the importance of these steps, as they can have important implications for the overall quality of the retrieved elevations. This especially true in high relief areas where small changes in the look angle, or introduced phase ambiguity, can produce large elevation errors ranging from 0-100 m in elevation (Brenner et al., 1983).

6 - Error analysis

To compute volume change errors for the three methods we divide the error budget into two main components (1) the observational error (ε_{obs}) and the interpolation error (ε_{int}). The observational error budget is estimated using the root-mean-square error (RMSE) of the difference between CryoSat-2 and airborne elevation change differences, as described in Section 5. The RMSE is estimated separately from the two different modes, with the total volume change error being computed as the RSS of standard error of the two modes, according to:

$$\varepsilon_{vol} = \sqrt{(\varepsilon_{lrm}\, A_{lrm})^2 + (\varepsilon_{sin}\, A_{sin})^2} \quad (12)$$

were A_{lrm} and A_{sin} are the corresponding areas covered by each mode. The ε_{lrm} and ε_{sin} are the standard errors of the LRM and SIN computed from the airborne validation data sets.

The observational elevation change error is estimated from the residual elevation change differences in Table-2 for the two methods. The RMSE from the LRM/SIN errors are computed using Gaussian error propagation producing an observational elevation change error (ε_{obs}). For the surface-fit and the crossover method the interpolation error is estimated as the RMS of the LSC uncertainty grid. The final elevation change error is then estimated by combing the two error sources using RSS according to:

$$\varepsilon_{dh/dt} = \sqrt{\left(\frac{\sigma_{obs}}{\sqrt{N}}\right)^2 + \left(\frac{\sigma_{int}}{\sqrt{N}}\right)^2} \quad (13)$$

Here, N is the number of uncorrelated grid-cells estimated from empirical semi-variogram analysis of the CryoSat-2 and airborne elevation change differences, and estimated according to:

$$N = \frac{A}{\rho_c^2} \quad (14)$$

were A is the total area of the Greenland Ice sheet (~1.7x10^6 km^2) and the correlation length ρ_c of 75 and 100 km for the LRM and SIN mode respectively.

Johan Nilsson 9/20/2016 10:06 AM
Comment [2]: NEED TO ADD VALIDATION OF RETRACKER HERE!

Johan Nilsson 9/20/2016 2:47 PM
Comment [3]: ADD A LONGER PARAGRAPH HERE SUMMARIZING THE SI

Johan Nilsson 9/22/2016 4:11 PM
Comment [4]: Rewrite! Sounds a bit strange the whole thing!

Johan Nilsson 9/23/2016 3:19 PM
Deleted: The impacts of the different SIN processing steps were quantified to determine the importance of the different processing steps in the reduction of RMSE. A simple case study over Barnes ice cap, on Baffin Island in the Canadian Arctic, was used to determine the impact of the processing. Barnes was chosen as it saw a major IceBridge ATM campaig ... [2]

Johan Nilsson 9/20/2016 10:06 AM
Deleted: (if appropriate)

Johan Nilsson 9/22/2016 4:06 PM
Deleted: the

Johan Nilsson 9/22/2016 4:05 PM
Deleted: e elevation

Johan Nilsson 9/22/2016 4:05 PM
Deleted: and

Johan Nilsson 9/22/2016 4:05 PM
Deleted: The overall error is then estimat ... [3]

Johan Nilsson 9/20/2016 10:06 AM
Deleted: area-weighted sum

Johan Nilsson 9/23/2016 9:47 AM
Deleted: the two components

Johan Nilsson 9/19/2016 3:31 PM
Deleted: $\left(\frac{A_{lrm}}{A_{tot}} \cdot \varepsilon_{lrm} + \frac{A_{sin}}{A_{tot}} \cdot \varepsilon_{sin}\right)$

Johan Nilsson 9/19/2016 3:31 PM
Deleted: $\cdot A_{tot}$

Johan Nilsson 9/20/2016 10:07 AM
Deleted: A_{tot} is the total area of the ice sheet,

Johan Nilsson 9/20/2016 10:07 AM
Deleted: summing to A_{tot}

Johan Nilsson 9/22/2016 4:09 PM
Deleted: CryoSat-2 - airborne

Johan Nilsson 9/22/2016 4:09 PM
Deleted: (

Johan Nilsson 9/22/2016 4:09 PM
Deleted:)

Johan Nilsson 9/22/2016 4:08 PM
Deleted: three

Johan Nilsson 9/20/2016 10:08 AM
Deleted: For the DEM-method only the ... [4]

Johan Nilsson 9/21/2016 6:12 PM
Deleted: 50

Johan Nilsson 9/19/2016 7:44 PM
Deleted: . ... [5]

7 – Results

The measured surface elevations from the two CryoSat-2 products (JPL vs. ESA) showed large differences in both accuracy and precision of the elevation measurements, as seen in Table-1. The average accuracy and precision for the LRM-mode from the two products showed values of 0.00 ± 0.43 m and -1.06 ± 0.89 m for the JPL and ESA products respectively. This corresponds to an average reduction in RMSE of 68% for the JPL product compared to the ESA LRM L2 data. Further, our product shows a lower residual slope error (seen in Figure-1c below ~0.5°), indicating a lower sensitivity to the degradation of performance as the surface slope increases.

Surface elevations generated from the SIN-mode showed the same type of improvement as for the LRM-mode. Here, an average accuracy and precision was found to be -0.52 ± 0.58 m and -0.90 ± 1.05 m for the JPL and ESA SIN elevation products respectively. This further corresponds to a reduction in the average RMSE of 27% for the JPL product compared to the ESA product. For the SIN-mode the JPL processing produces a slightly lower residual slope error, compared to the ESA processor (seen in Figure-1c above ~0.5°).

Larger improvements can be observed if separating the RMSE into its mean and standard deviation, corresponding to the accuracy and precision of the measurements. Using these definitions the analysis found that there is a 45% and 52% increase in precision for the SIN and LRM mode respectively, compared to the ESA L2 product, and a 42% and 99% improvement in accuracy for the respective modes.

The estimated surface elevation changes generated from the surface-fit method also showed improvement in the estimated accuracy and precision, as seen in Table-2. Here, a overall improvement in RMSE of 55% and 40% in the LRM and SIN mode, respectively, was found when comparing against ESA L2 generated elevation changes from the same method. The average accuracy and precision, compared to ATM generated elevation changes, was found to be 0.11 ± 0.67 m (LRM) and 0.30 ± 0.58 m (SIN) for the JPL derived changes. This

660 compared to 0.25 ± 1.51 m (LRM) and 0.34 ± 1.06 m (SIN) for the ESA derived changes. This
661 corresponds to an increase in elevation change accuracy of 56% and 12% for the LRM and
662 SIN-mode, respectively, for the JPL product compared to ESA L2 elevation changes. The
663 estimated elevation changes also show an increase in precisions for the JPL product of 56%
664 and 45% for the LRM and SIN-mode, respectively, compared to its ESA counterpart.

665 The implementation of the LMG SIN retracking algorithm was found to reduce noise in
666 the retrieved surface elevations compared to conventional threshold retracking. Though roughly
667 comparable in accuracy, the LMG shows overall higher precision over all comparable leading
668 edge thresholds. The adaptive nature of the algorithm provides improved estimates of surface
669 elevation and gives good trade-off between accuracy and precision.

670 The 20% threshold retracker implemented in the LRM-mode was also found to provide
671 improved estimates of surface elevation (both in accuracy and precision) compared to the
672 model-based ESA-L2 retracker. Further, it also showed lower sensitivity to the 2012 melt event,
673 due to the lower threshold used on the leading edge of the waveform.

674 The estimated elevation changes of the Greenland Ice Sheet, excluding the peripheral
675 glaciers, over the period January 2011 to January 2015 show significant differences between
676 products (JPL and ESA) in both spatial patterns and the total magnitude (Figures 3 & 4). The
677 estimated volume change rate from the surface-fit method is -289 ± 20 $km^3 a^{-1}$ for the JPL-
678 product and -224 ± 38 $km^3 a^{-1}$ for the ESA-product with a mean difference of 65 $km^3 a^{-1}$. The
679 surface-fit and crossover-method produced on the order of ~20 million and ~2.5 million usable
680 elevation changes, respectively, providing high spatial sampling. Due to the constraint put into
681 the JPL processor the ESA L2 data produced slightly more surface-fit observations (~10%), as
682 more surface elevations were accepted.

683 The ESA product produces a more positive elevation change pattern, which can be
684 attributed to the 2012 melt event that introduced a large positive bias with a magnitude of ~0.5
685 m (Nilsson et al., 2015). Larger differences in the marginal areas for the surface-fit methods are

Johan Nilsson 9/27/2016 10:58 AM
Deleted: the

Johan Nilsson 9/27/2016 10:59 AM
Formatted: Not Highlight

Johan Nilsson 9/27/2016 10:56 AM
Deleted: This is exemplified over the Jakobshavn Isbræ area of the Greenland Ice Sheet (Figure), where LMG and a leading edge threshold retracker were compared

Johan Nilsson 9/27/2016 10:56 AM
Deleted: .

Johan Nilsson 9/27/2016 10:56 AM
Deleted: has a 32% improvement in precision when, compared against elevations from airborne laser altimetry

Johan Nilsson 9/27/2016 10:58 AM
Deleted: .

Johan Nilsson 9/27/2016 12:33 PM
Deleted: 2

Johan Nilsson 9/27/2016 12:33 PM
Deleted: 3

Johan Nilsson 9/22/2016 11:37 AM
Deleted: 16

Johan Nilsson 9/22/2016 11:37 AM
Deleted: 1

also observed. These are particularly noticeable in eastern Greenland (near 73.5 degrees in latitude Figure 3) where the ESA data shows marginal areas of rapid thinning that are not visible in the JPL solution. The positive signal detected in the interior of the ESA surface-fit-solution can also be found in the basin time series, correlating well with the timing of the summer of 2012 melt event. These results are in agreement with earlier work demonstrating the sensitivity of the ESA retracker to the changes in the volume/surface scattering ratio (Nilsson et al., 2015).

The two volume change methods produce consistent results from JPL derived elevation changes, with a difference of around 1 $km^3 a^{-1}$. The spread between volume change methods is larger (50 $km^3 a^{-1}$) when using ESA L2 data. The larger discrepancy can mostly related to the sensitivity of the various methods to the melt event. The surface-fit method produces the most negative number (least affected by the melt event and the lowest estimated error) and is therefore taken as the most reliable estimate for both the JPL and ESA solution.

Comparing the estimated volume change to other studies using CryoSat-2 we find that the JPL product is less negative than that estimated by Helm et al. (2014): -375 ± 24 $km^3 a^{-1}$. This difference can be attributed to difference in processing methodology and to the different epoch of the data used by Helm et al. (2014) of January 2011 to January 2014. Using the corresponding epoch the JPL data gives a volume change estimate, based on the surface-fit method, of -353 ± 21 $km^3 a^{-1}$, well within the stated uncertainty of Helm et al. (2014).

To examine the regional behavior of volume change estimates of the Greenland Ice Sheet, gridded values from the three methods were divided into 8-drainage basins according to Zwally et al. (2012). When analyzing the volume change time-series at the basin scale clear differences can be observed in the annual and inter-annual behaviors (Figure 4). The northern and interior basins (1, 2, 7, 8) all exhibit large differences (Table 4: 0 - 30 $km^3 a^{-1}$) in the estimated volume change rates due to changes in the scattering regime resulting from the 2012 melt event. In the majority of the southern basins (4, 5, 6, 7), located in areas with higher

Johan Nilsson 9/23/2016 3:24 PM
Deleted: 2

Johan Nilsson 9/20/2016 10:12 AM
Deleted: can also be found in the ESA DEM-solution

Johan Nilsson 9/16/2016 5:13 PM
Formatted: Highlight

Johan Nilsson 9/20/2016 10:13 AM
Deleted: three

Johan Nilsson 9/20/2016 10:15 AM
Deleted: less than

Johan Nilsson 9/20/2016 10:14 AM
Deleted: 7

Johan Nilsson 9/23/2016 3:26 PM
Deleted: 3

precipitation, both products show good agreement in both trends and seasonal amplitude estimated from the surface-fit method.

The amplitude of the seasonal signal (Equation 4) estimated from the surface-fit (SF) method show large differences in both magnitude and spatial variability (Figure 5). For the surface-fit method a difference in amplitude of 54% is observed between the ESA and JPL products, corresponding to area-averaged amplitude of 0.17 m or the JPL product and of 0.37 m for ESA product. The comparison with ICESat derived amplitudes from 2003-2009 estimated in (Sasgen et al., 2012) using the same methodology as used here produced an area-averaged amplitude of 0.13 m, which is in good agreement with the JPL derived amplitude. This agreement is also spatially consistent, as seen in (Figure 5), indicating low sensitivity to seasonal changes in scattering regime of the upper snowpack. The observed difference in amplitude bias, taking ICESat as the true surface amplitude while acknowledging that no inter-campaign bias has been applied and the differences in epochs, is 0.03 ± 0.13 m for the JPL product and 0.21 ± 0.27 m for the ESA product. The smallest differences are observed at high altitudes above 2000 m a.s.l., where the three data sets show almost constant amplitude of 0.1 m (ICE/JPL) and 0.2 m (ESA), providing a factor of two larger amplitude for the ESA product. Below 2000 m a.s.l., corresponding well to the equilibrium-line-altitude (ELA) of the Greenland Ice Sheet, a rapid increase in amplitude is observed for all products. This is especially true for the ESA product, which increases its magnitude by a factor of two.

Analyzing the amplitude patterns on a regional drainage basin level (Figure 5c) we find good agreement between JPL CryoSat-2 and ICESat amplitude with ESA data producing consistently larger amplitudes. Regionally, the highest amplitudes can be observed in the SE of Greenland in basins (3,4,5) and are consistent with regional precipitation patterns that show high average precipitation in these areas (Bales et al., 2009; Ettema et al., 2009).

The seasonal phase of the peak in amplitude of the seasonal cycle is shown in (Figures 5b and 5c) and shows generally good agreement between the two products, providing the

Johan Nilsson 9/20/2016 10:15 AM
Deleted: DEM-

Johan Nilsson 9/20/2016 10:16 AM
Formatted: Not Highlight

Johan Nilsson 9/20/2016 10:59 AM
Deleted: 5

Johan Nilsson 9/20/2016 10:59 AM
Deleted: 5

Johan Nilsson 9/20/2016 11:00 AM
Deleted: 5

762 timing of the maximum of the accumulation signal, before the onset of melt, to the months of
763 June/July for both JPL and ESA CryoSat-2 data sets. The ICESat derived seasonal phase
764 shows a higher dependence on elevation where the maximum of the accumulation signal is
765 found in late May below 2000 m and late July/August above 2000 m in elevation. The ICESat
766 discrepancies from the CryoSat-2 data are found in specific basins. Disagreements between the
767 retrieved phase of the peak amplitude from Cryosat-2 and ICESat data are due to differences in
768 temporal sampling as discussed in more detail in Section 8.1.

769 We used ICESat and CryoSat-2 derived surface heights to generate time series over
770 three regions in Northeast area of Greenland (Zachariæ Isstrøm, Nioghalvfjerdsfjorden and
771 Storstrømmen glaciers) for comparison purposes These areas have in recent time shown large
772 and rapid changes, which has been noted by, e.g., Khan et al. (2014). The selected areas were
773 defined using hydrological basins derived by Lewis and Smith (2009), seen in (Figure 6), and
774 were further divided into smaller areas around the termini to highlight performance for areas of
775 rapid change. The ICESat and CryoSat-2 surface heights were then used to generate annual
776 time-series from 2003-2015 using (Equation 6) in the surface fit method. The estimated 12 year
777 time series show overall comparable elevation change rates over both time periods, especially
778 in the terminus areas, providing confidence that CryoSat-2 can actually monitor changes in
779 these areas.
780
781
782
783
784

Johan Nilsson 9/20/2016 11:00 AM
Deleted: 6

8 - Discussion

The CryoSat-2 processing methodology presented here is found to produce accurate and precise measurements of ice sheet elevation and elevation change. The main improvements have been introduced in the SIN processor with the inclusion of a new type of land ice retracker (LMG), advanced phase filtering and the inclusion of a phase ambiguity correction scheme. This processing approach decreased the RMSE in the surface height retrieval by approximately 27% (45% and 42% improvement in precision and accuracy). This improvement further propagated into the quality of the estimated elevation changes for the SIN-mode, with the same magnitude of improvement (Table-2). The described SIN-processing also generated surface elevations and elevation changes with lower sensitivity to the local surface slope, indicating a higher degree of accuracy in the geo-location and surface range estimation.

The SIN processing methodology further includes a phase filtering and phase ambiguity correction scheme. Visual inspections of a large number of tracks have shown more coherent estimation of the surface locations in our product and further the implementation of the phase-ambiguity correction greatly reduced the number of track offsets. It was also noted that a relatively course DEM (~1 km) could be used to resolve phase ambiguities. The detection and correction of phase ambiguities are relatively straightforward and rely mostly on the relative accuracy of the DEM. The implementation of the phase ambiguity correction is particularly important when monitoring smaller ice caps and outlet glaciers, where frequent and large track offsets can bias the estimation of the underlying topography.

Johan Nilsson 9/27/2016 11:52 AM
Deleted: The statistical effects of these corrections have been analyzed over the Barnes Ice Cap on Ellesmere Island in the Canadian Arctic and are available in Table S1.

The new LRM processing methodology focused on optimal retrieval of surface elevations over the interior parts of the ice sheet. Here the choice of retracking threshold has proven to be the critical factor to acquire high quality surface elevations and elevation changes. The choice of 20% leading edge threshold level reduced the sensitivity to changes in the scattering regime for low slope, high elevation areas. The functional-based retracking algorithm

used in the ESA LRM processor corresponds roughly to a 50% threshold level (Wingham et al., 2006a), which appears to suffer from a higher sensitivity to changes in the scattering properties (volume scattering) of the near-surface firn, as the range is reference higher up (later in time) on the leading edge of the waveform. This effect can be seen in (Figure 2a), and that the observed negative elevation bias (Table-1) for ESA-LRM (-1.0 m) fit well with the bias for the 50% LRM threshold value shown in Figure 2a. This makes the algorithm more sensitive to annual and sub-annual changes in snow-packs volume/surface scattering ratio, which can produce spurious changes in elevation due to changes in the near surface dielectric properties. This is clearly shown in patterns of ESA product derived elevation changes (Figure 3) where a large elevation bias was introduced by the 2012-melt event (Nilsson et al., 2015a). The 20% threshold is less sensitive to these types of changes (Table 1 & 2) and is in agreement with previous work that has demonstrated that the 20% threshold best represents the mean surface inside the footprint when exposed to a combination of surface and volume scattering (Davis, 1997).

Surface elevation changes, derived from multi-temporal radar altimetry observations, are typically corrected for their correlation to changes in the radar waveform shape. This is to reduce the effect of changes in the volume/surface scattering ratio of the ice sheets surface (Davis, 2005; Flament and Rémy, 2012; Wingham et al., 2006b; Zwally et al., 2005). This inherently adds to the complexity of the processing and analysis, introducing new biases and error sources in the estimated parameters. For the processing approach presented here many of these steps can be omitted or reduced, as they are an inherent part of the improved waveform retracking. There have been attempts to remove spurious step-changes in elevation resulting from sudden changes in surface scattering characteristics (caused by the 2012 melt event) apparent in the ESA Baseline-B L2 data through post-processing strategies (Nilsson et al., 2015c), but such approaches spread the bias over a longer period of time making the "jumps" less noticeable in the time series by removing the step-change but introduces longer-

Johan Nilsson 9/23/2016 3:26 PM
Deleted: S

Johan Nilsson 9/23/2016 3:26 PM
Deleted: 1

Johan Nilsson 9/23/2016 3:38 PM
Deleted: S

Johan Nilsson 9/23/2016 3:38 PM
Deleted: 1

Johan Nilsson 9/23/2016 3:25 PM
Deleted: 2b

timescale bias of equal magnitude as the scattering layer is buried by less reflective snow and low-density firn.

The result of the validation procedure shows a larger slope dependent bias in the ESA data, both in the elevation and elevation changes (Figure 1). This is especially true for the surface elevations, which can be seen in the figures of precision and accuracy (Figure 1a and 1c), where both figures show clear linear slope for the ESA surface heights. In comparison, estimated elevations from JPL-product show relatively stable statistics over the entire slope range above 0.2°. The validation of the estimated surface elevation changes, seen in (Figure 1b) and (Figure 1d), shows the effect of the 2012 melt event on the ESA derived elevation changes below 0.2°. Further, the accuracy of the ESA derived changes show a clear negative trend as function of increased surface slope. The derived precision of the surface elevation change increases dramatically above 0.5°, as more complex topography is measured.

The JPL CryoSat-2 processing methodology produces seasonal amplitudes that are in good agreement with those derived from ICESat data, further indicating the processors abilities to track real and physical changes of the ice sheets surface. The current ESA implementation produces noisier estimates of elevation change, as indicated by the larger standard deviations of the residuals in the ESA solutions for the surface-fit and crossover-method. Figure 5 further shows an amplitude bias in the ESA data compared to the corresponding ICESat reference amplitudes. The bias is constant above the Greenland ELA located around 2000 m in altitude but increases linearly as elevations decrease below this. The linear increase in amplitude seems to be connected to the higher and more variable precipitation in the ablation zone where changes in the variable snow cover produces changes in apparent surface height. This is less prominent for the JPL SIN and LRM retrackers. The estimated seasonal phase in Figure 5c and 5d show that both JPL and ESA CryoSat-2 elevation products can adequately resolve the seasonal maximum of the accumulation signal. Both products provide a timing of the maximum to the month of July over the entire ice sheet, independent of elevation. Assessing the CryoSat-

Johan Nilsson 9/22/2016 4:18 PM
Deleted:

Johan Nilsson 9/22/2016 4:18 PM
Deleted: and Table 1 & 2

Johan Nilsson 9/20/2016 11:00 AM
Deleted: 5

Johan Nilsson 9/20/2016 11:00 AM
Deleted: 5

875 2 derived maximum one does however notice a difference between CryoSat-2 and the
876 reference ICESat dataset. This constitutes roughly a ±1 month difference depending on the
877 elevation and the location. The cause of this difference can be attributed to the temporal
878 sampling of the ICESat mission. During the mission, due to degraded laser lifespan, data was
879 only collected in campaign mode during the spring and winter times corresponding to roughly
880 two months of measurements for each period. When the CryoSat-2 data was resampled to
881 coincide with the ICESat temporal sampling the same elevation and spatial pattern in the phase
882 of the maximum seasonal amplitude was observed as determined from the ICESat data. No
883 corresponding change in amplitude was observed. To mimic the temporal sampling of ICESat
884 the each year of the CryoSat-2 data was resampled using the total number of unique months in
885 the ICESat campaign record. This as the specific months used in the ICESat sampling changes
886 with different campaigns.

887 The two independent methods used to estimate the volume change of the Greenland Ice
888 Sheet produce consistent volume change estimates. This was especially true for volume
889 changes derived from the JPL elevations, with a discrepancy of less than 1 $km^3 a^{-1}$ between
890 methods. The two methods provided the same estimate of integrated volume change but the
891 use of the surface-fit is recommended as it produces higher spatial sampling compared to the
892 crossover-method and lower errors. The good agreement between the methods further
893 indicates a strong reliability in the estimated volume change rates of the Greenland Ice Sheet
894 over the four-year period. It also shows the ability of CryoSat-2 to capture both small and large-
895 scale spatial patterns in the rugged topography along the coastline and in the interior of
896 Greenland. This is especially true in the major outlet glacier systems (e.g., Zachariæ Isstrøm,
897 Nioghalvfjerdsfjorden and Storstrømmen).

898 Studying the northern parts of the Greenland Ice Sheet we find that CryoSat-2 captures
899 both intricate and complex behavior in the marginal areas of the ice sheet. This is exemplified in
900 the NE regions of Greenland (Figure 6) near Zachariæ Isstrøm, Nioghalvfjerdsfjorden and

Johan Nilsson 9/20/2016 10:19 AM
Deleted: three

Johan Nilsson 9/20/2016 10:19 AM
Deleted: 7

Johan Nilsson 9/20/2016 10:19 AM
Deleted: All

Johan Nilsson 9/20/2016 10:19 AM
Deleted: three

Johan Nilsson 9/20/2016 10:20 AM
Deleted: i.e.

Johan Nilsson 9/19/2016 1:22 PM
Deleted: Zachariae Isstrøm, Nioghalvfjerdsbrae (N79) and Storstrømmen

Johan Nilsson 9/20/2016 11:01 AM
Deleted: 6

Johan Nilsson 9/19/2016 1:23 PM
Deleted: Nioghalvfjerdsbrae

Storstrømmen, which all show complex and localized patterns of elevation change. Here, Nioghalvfjerdsbrae shows very small changes in elevation during the observational time-span, while Zachariae Isstrøm, its major neighbor shows large negative trends in elevation change. The observed behavior agrees with the observations made in recent studies by Khan et al. (2014) and Mouginot et al. (2015) who document rapid retreat and drawdown of the ice-front position of the two systems beginning in 2012. Storstrømmen outlet glacier system also appears to show signs of rapid thinning at low elevations near the ice-front position while a large positive signal is observed roughly 100 km upstream of the terminus. This pattern has also been observed by Joughin et al., (2010) and Thomas et al., (2009), using airborne altimetry and surface velocity mapping. Rates of elevation change from ICESat and CryoSat-2 data show good agreement in basin-scale trends (Figure 6b,c).

Johan Nilsson 9/18/2016 7:36 PM
Deleted: by

Johan Nilsson 9/20/2016 9:51 AM
Deleted: (

Johan Nilsson 9/20/2016 9:51 AM
Deleted: ;

Johan Nilsson 9/20/2016 9:49 AM
Deleted: .

Johan Nilsson 9/20/2016 11:01 AM
Deleted: 6

The observed volume change rates estimated from this study are within the range of previous studies, ranging from -186 to -309 $km^3\ a^{-1}$ for the time period 2003-2009, summarized by Csatho et al. (2014). A more recent study by Helm et al. (2014: -375 ± 24 $km^3\ a^{-1}$) agrees within uncertainties when differences in observation periods (2011 – 2014 vs. 2011 - 2015) are taken into accounted. Assuming no changes in firn air content over respective study periods and an ice density of 917 kg m^{-3} we compare estimated changes with corresponding estimates of mass change our estimated rate of Greenland glacier volume change. An assessment of changes in firn air content is out of the scope of this paper. Velicogna et al. (2014) estimated mass loss using the Gravity Recovery and Climate Experiment satellites (GRACE) over the time-period 2003-2013 provided (converted from mass) a rate of -305 ± 63 $km^3\ a^{-1}$ for the Greenland which is inclusive of changes in Ice Sheet and peripheral glacier ice mass (–41 ± 8 $km^3\ a^{-1}$, Gardner et al., 2013). The estimated volume change of -265 $km^3\ a^{-1}$ from Csatho et al. (2014) and the estimated rate of -305 $km^3\ a^{-1}$ from Velicogna et al. (2014) spans our estimated rate of -289 $km^3\ a^{-1}$.

9 – Summary and Conclusion

We conclude that the use of an adaptive retracker for the SIN-mode, based on the maximum gradient method, and the use of 20% threshold retracker for the LRM-mode provide improved performance to the retracker currently used for the ESA L2 elevation products. It is further important, especially for the SIN-mode, to apply a leading edge discriminator to identify and track the leading edge of the waveform. The functional model currently employed in the ESA processor has, to the author's knowledge, no such discriminator currently implemented. This is important in the SIN-mode, as it often contains multiple surface returns. The single-return model applied in the ESA processor will here have issues fitting a waveform containing multiple surface returns resulting in retrack jitter (Helm et al., 2014).

Using the new CryoSat-2 processing methodology for the LRM and SIN-mode we determine the volume change of the Greenland Ice Sheet to be -289 ± 20 $km^3 a^{-1}$ during the period January 2011 to January 2015. The validation against airborne ATM surface elevations and elevation changes showed an average improvement in the RMSE of the measured elevations of 68% and 27% for the LRM and SIN mode respectively compared to ESA Baseline-B L2 products. The new methodology also provide improved elevation changes with an reduction in RMSE of 55% and 40% for the LRM and SIN mode respectively, compared to their ESA L2 derived counterparts.

Johan Nilsson 9/22/2016 11:37 AM
Deleted: 16

The methodology also showed less sensitivity to changes in near-surface scattering properties than equivalent ESA products. The new processing methodology showed little effect of slope-induced errors, providing better performance in the marginal areas of the ice sheets. These improvements to the CryoSat-2 processing mitigate the need for post-processing to correct correlations between changes in surface elevation and changes in the waveform shape (i.e. backscatter and leading edge width etc.) that can introduce biases and add to the complexity of the processing and analysis.

The presented CryoSat-2 processing methodology provides a lower intrinsic error in the measured elevation, elevation change and volume change estimates, all of which will facilitate improved understanding of the geophysical process leading to changes in land ice elevation. Given the release of the ESA Baseline-C, which provides improved corrections and processing mainly for the L1B product, further improvements are expected in the near future.

The complete set of grids used in this study is available for the public from the main author (J.Nilsson) upon request and are provided in geotiff format.

Acknowledgement

We are deeply thankful for the guidance of Laurence Gray and support of David Burgess. We also thank Sebastian Bjerregaard Simonsen for very fruitful discussions. Further, we would also thank and acknowledge Frank Paul at the University of Zurich for providing us with polygon-outlines of the Greenland Ice Sheet and to the European Space Agency for providing their CryoSat-2 L1b product. We thank the editor E. Berthier , the reviewer L. Schröder and the anonymous reviewer for valuable comments, which greatly helped to improve this manuscript. This work was supported by funding from the NASA Cryosphere program. The research was conducted at the Jet Propulsion Laboratory, California Institute of Technology under contract with NASA.

Johan Nilsson 9/27/2016 1:14 PM
Deleted: pending

Johan Nilsson 9/26/2016 10:34 AM
Deleted: his plotting software and

Johan Nilsson 9/19/2016 7:39 PM
Deleted:

992 References

993 Abulaitijiang, A., Andersen, O. B. and Stenseng, L.: Coastal sea level from inland CryoSat-2
994 interferometric SAR altimetry, Geophys. Res. Lett., 42(6), 1841–1847,
995 doi:10.1002/2015GL063131, 2015.
996 Arthern, R., Wingham, D. and Ridout, A.: Controls on ERS altimeter measurements over ice
997 sheets: Footprint-scale topography, backscatter fluctuations, and the dependence of microwave
998 penetration depth on satellite orientation, J. Geophys. Res. Atmos., 106(D24), 33471–33484,
999 doi:10.1029/2001JD000498, 2001.
1000 Bales, R. C., Guo, Q., Shen, D., McConnell, J. R., Du, G., Burkhart, J. F., Spikes, V. B., Hanna,
1001 E. and Cappelen, J.: Annual accumulation for Greenland updated using ice core data developed
1002 during 2000-2006 and analysis of daily coastal meteorological data, J. Geophys. Res. Atmos.,
1003 114(6), doi:10.1029/2008JD011208, 2009.
1004 Bamber, J. L.: Ice sheet altimeter processing scheme, Int. J. Remote Sens., 15(4), 925–938,
1005 doi:10.1080/01431169408954125, 1994.
1006 Brenner, A. C., Blndschadler, R. A., Thomas, R. H. and Zwally, H. J.: Slope-induced errors in
1007 radar altimetry over continental ice sheets, J. Geophys. Res., 88(C3), 1617,
1008 doi:10.1029/JC088iC03p01617, 1983.
1009 Brenner, A. C. ., DiMarzio, J. P. . and Zwally, H. J. .: Precision and accuracy of satellite radar
1010 and laser altimeter data over the continental ice sheets, IEEE Trans. Geosci. Remote Sens.,
1011 45(2), 321–331, doi:10.1109/TGRS.2006.887172, 2007.
1012 Csatho, B. M., Schenk, A. F., van der Veen, C. J., Babonis, G., Duncan, K., Rezvanbehbahani,
1013 S., van den Broeke, M. R., Simonsen, S. B., Nagarajan, S. and van Angelen, J. H.: Laser
1014 altimetry reveals complex pattern of Greenland Ice Sheet dynamics., Proc. Natl. Acad. Sci. U. S.
1015 A., 111(52), 18478–83, doi:10.1073/pnas.1411680112, 2014.
1016 Davis, C. H.: Surface and volume scattering retracking algorithm for ice sheet satellite altimetry,

IEEE Trans. Geosci. Remote Sens., 31(4), 811–818, doi:10.1109/36.239903, 1993.

Davis, C. H.: A robust threshold retracking algorithm for measuring ice-sheet surface elevation change from satellite radar altimeters, IEEE Trans. Geosci. Remote Sens., 35(4), 974–979, doi:10.1109/36.602540, 1997.

Davis, C. H.: Snowfall-Driven Growth in East Antarctic Ice Sheet Mitigates Recent Sea-Level Rise, Science (80-.)., 308(5730), 1898–1901, doi:10.1126/science.1110662, 2005.

Davis, C. H. and Ferguson, A. C.: Elevation change of the antarctic ice sheet, 1995-2000, from ERS-2 satellite radar altimetry, IEEE Trans. Geosci. Remote Sens., 42(11), 2437–2445, doi:10.1109/TGRS.2004.836789, 2004.

Ettema, J., Van Den Broeke, M. R., Van Meijgaard, E., Van De Berg, W. J., Bamber, J. L., Box, J. E. and Bales, R. C.: Higher surface mass balance of the Greenland ice sheet revealed by high-resolution climate modeling, Geophys. Res. Lett., 36(12), 1–5, doi:10.1029/2009GL038110, 2009.

Flament, T. and Rémy, F.: Dynamic thinning of Antarctic glaciers from along-track repeat radar altimetry, J. Glaciol., 58(211), 830–840, doi:10.3189/2012JoG11J118, 2012.

Galin, N., Wingham, D. J., Cullen, R., Fornari, M., Smith, W. H. F. and Abdalla, S.: Calibration of the CryoSat-2 interferometer and measurement of across-track ocean slope, IEEE Trans. Geosci. Remote Sens., 51(1), 57–72, doi:10.1109/TGRS.2012.2200298, 2013.

Gardner, A. S., Moholdt, G., Cogley, J. G., Wouters, B., Arendt, A. a, Wahr, J., Berthier, E., Hock, R., Pfeffer, W. T., Kaser, G., Ligtenberg, S. R. M., Bolch, T., Sharp, M. J., Hagen, J. O., van den Broeke, M. R. and Paul, F.: A reconciled estimate of glacier contributions to sea level rise: 2003 to 2009., Science, 340(6134), 852–7, doi:10.1126/science.1234532, 2013.

Gray, L., Burgess, D., Copland, L., Cullen, R., Galin, N., Hawley, R. and Helm, V.: Interferometric swath processing of Cryosat data for glacial ice topography, Cryosph., 7(6), 1857–1867, doi:10.5194/tc-7-1857-2013, 2013.

Gray, L., Burgess, D., Copland, L., Demuth, M. N., Dunse, T., Langley, K. and Schuler, T. V.:

CryoSat-2 delivers monthly and inter-annual surface elevation change for Arctic ice caps, Cryosph., 9(5), 1895–1913, doi:10.5194/tc-9-1895-2015, 2015.

Helm, V., Humbert, A. and Miller, H.: Elevation and elevation change of Greenland and Antarctica derived from CryoSat-2, Cryosph., 8(4), 1539–1559, doi:10.5194/tc-8-1539-2014, 2014.

Herzfeld, U. C.: Least-squares collocation, geophysical inverse theory and geostatistics: a bird's eye view, Geophys. J. Int., 111(2), 237–249, doi:10.1111/j.1365-246X.1992.tb00573.x, 1992.

Howat, I. M., Smith, B. E., Joughin, I. and Scambos, T. A.: Rates of southeast Greenland ice volume loss from combined ICESat and ASTER observations, Geophys. Res. Lett., 35(17), 1–5, doi:10.1029/2008GL034496, 2008.

Howat, I. M., Negrete, A. and Smith, B. E.: The Greenland Ice Mapping Project (GIMP) land classification and surface elevation data sets, Cryosph., 8(4), 1509–1518, doi:10.5194/tc-8-1509-2014, 2014.

Joughin, I., Smith, B. E., Howat, I. M., Scambos, T. and Moon, T.: Greenland flow variability from ice-sheet-wide velocity mapping, J. Glaciol., 56(197), 415–430, doi:10.3189/002214310792447734, 2010.

Keith Raney, R.: The delay/doppler radar altimeter, IEEE Trans. Geosci. Remote Sens., 36(5), 1578–1588, doi:10.1109/36.718861, 1998.

Khan, S. a, Kjaer, K. H., Bevis, M., Bamber, J. L., Wahr, J., Kjeldsen, K. K., Bjork, A. a, Korsgaard, N. J., Stearns, L. a, van den Broeke, M. R., Liu, L., Larsen, N. K. and Muresan, I. S.: Sustained mass loss of the northeast Greenland ice sheet triggered by regional warming, Nat. Clim. Chang., 4(4), 292–299, doi:10.1038/nclimate2161, 2014.

Khvorostovsky, K. S.: Merging and Analysis of Elevation Time Series Over Greenland Ice Sheet From Satellite Radar Altimetry, IEEE Trans. Geosci. Remote Sens., 50(1), 23–36, doi:10.1109/TGRS.2011.2160071, 2012.

Krabill, W. B., Abdalati, W., Frederick, E. B., Manizade, S. S., Martin, C. F., Sonntag, J. G.,

1069 Swift, R. N., Thomas, R. H. and Yungel, J. G.: Airborne laser altimetry mapping of the
1070 Greenland ice sheet : application to mass balance assessment, J. Geodyn., 34, 357–376,
1071 doi:10.1016/s0264-3707(02)00048-0, 2002.
1072 Lacroix, P., Dechambre, M., Legrésy, B., Blarel, F. and Rémy, F.: On the use of the dual-
1073 frequency ENVISAT altimeter to determine snowpack properties of the Antarctic ice sheet,
1074 Remote Sens. Environ., 112, 1712–1729, doi:10.1016/j.rse.2007.08.022, 2008.
1075 Lewis, S. M. and Smith, L. C.: Hydrologic drainage of the Greenland Ice Sheet, Hydrol.
1076 Process., 23(14), 2004–2011, doi:10.1002/hyp.7343, 2009.
1077 Moholdt, G., Nuth, C., Hagen, J. O. and Kohler, J.: Recent elevation changes of Svalbard
1078 glaciers derived from ICESat laser altimetry, Remote Sens. Environ., 114(11), 2756–2767,
1079 doi:10.1016/j.rse.2010.06.008, 2010.
1080 Mouginot, J., Rignot, E., Scheuchl, B., Fenty, I., Khazendar, A., Morlighem, M., Buzzi, A. and
1081 Paden, J.: Fast retreat of Zachariae Isstrom, northeast Greenland, Science (80-.)., 350(6266),
1082 1357–1361, doi:10.1126/science.aac7111, 2015.
1083 Nilsson, J., Vallelonga, P., Simonsen, S. B., Sørensen, L. S., Forsberg, R., Dahl-Jensen, D.,
1084 Hirabayashi, M., Goto-Azuma, K., Hvidberg, C. S., Kjaer, H. A. and Satow, K.: Greenland 2012
1085 melt event effects on CryoSat-2 radar altimetry, Geophys. Res. Lett., 42(10), 3919–3926,
1086 doi:10.1002/2015GL063296, 2015a.
1087 Nilsson, J., Sandberg Sørensen, L., Barletta, V. R. and Forsberg, R.: Mass changes in Arctic ice
1088 caps and glaciers: implications of regionalizing elevation changes, Cryosph., 9(1), 139–150,
1089 doi:10.5194/tc-9-139-2015, 2015b.
1090 Remy, F., Mazzega, P., Houry, S., Brossier, C. and Minster, J. F.: Mapping of the topography of
1091 continental ice by inversion of satellite-altimeter data, J. Glaciol., 35(119), 98–107,
1092 doi:10.3189/002214389793701419, 1989.
1093 Remy, F., Flament, T., Blarel, F. and Benveniste, J.: Radar altimetry measurements over
1094 antarctic ice sheet: A focus on antenna polarization and change in backscatter problems, Adv.

Sp. Res., 50(8), 998–1006, doi:10.1016/j.asr.2012.04.003, 2012.

Sasgen, I., van den Broeke, M., Bamber, J. L., Rignot, E., Sørensen, L. S., Wouters, B., Martinec, Z., Velicogna, I. and Simonsen, S. B.: Timing and origin of recent regional ice-mass loss in Greenland, Earth Planet. Sci. Lett., 333–334, 293–303, doi:10.1016/j.epsl.2012.03.033, 2012.

Shepherd, A., Ivins, E. R., A, G., Barletta, V. R., Bentley, M. J., Bettadpur, S., Briggs, K. H., Bromwich, D. H., Forsberg, R., Galin, N., Horwath, M., Jacobs, S., Joughin, I., King, M. A., Lenaerts, J. T. M., Li, J., Ligtenberg, S. R. M., Luckman, A., Luthcke, S. B., McMillan, M., Meister, R., Milne, G., Mouginot, J., Muir, A., Nicolas, J. P., Paden, J., Payne, A. J., Pritchard, H., Rignot, E., Rott, H., Sorensen, L. S., Scambos, T. A., Scheuchl, B., Schrama, E. J. O., Smith, B., Sundal, A. V., van Angelen, J. H., van de Berg, W. J., van den Broeke, M. R., Vaughan, D. G., Velicogna, I., Wahr, J., Whitehouse, P. L., Wingham, D. J., Yi, D., Young, D. and Zwally, H. J.: A Reconciled Estimate of Ice-Sheet Mass Balance, Science (80-.)., 338(6111), 1183–1189, doi:10.1126/science.1228102, 2012.

Sørensen, L. S., Simonsen, S. B., Nielsen, K., Lucas-Picher, P., Spada, G., Adalgeirsdottir, G., Forsberg, R. and Hvidberg, C. S.: Mass balance of the Greenland ice sheet (2003-2008) from ICESat data - The impact of interpolation, sampling and firn density, Cryosphere, 5(1), 173–186, doi:10.5194/tc-5-173-2011, 2011.

Sørensen, L. S., Simonsen, S. B., Meister, R., Forsberg, R., Levinsen, J. F. and Flament, T.: Envisat-derived elevation changes of the Greenland ice sheet, and a comparison with ICESat results in the accumulation area, Remote Sens. Environ., 160, 56–62, doi:10.1016/j.rse.2014.12.022, 2015.

Thomas, R., Frederick, E., Krabill, W., Manizade, S. and Martin, C.: Recent changes on Greenland outlet glaciers, J. Glaciol., 55(189), 147–162, doi:10.3189/002214309788608958, 2009.

Velicogna, I., Sutterley, T. C. and Van Den Broeke, M. R.: Regional acceleration in ice mass

loss from Greenland and Antarctica using GRACE time-variable gravity data, Geophys. Res. Lett., 41(22), 8130–8137, doi:10.1002/2014GL061052, 2014.

Wenlu Qi and Braun, A.: Accelerated elevation change of Greenland's Jakobshavn glacier observed by ICESat and IceBridge, IEEE Geosci. Remote Sens. Lett., 10(5), 1133–1137, doi:10.1109/LGRS.2012.2231954, 2013.

Wingham, D. J., Rapley, C. G. and Griffiths, H.: New Techniques in Satellite Altimeter Tracking Systems, in Proceedings of the IGARSS Symposium, Zurich, pp. 1339–1344, ESA SP-254, Zurich., 1986.

Wingham, D. J., Francis, C. R., Baker, S., Bouzinac, C., Brockley, D., Cullen, R., de Chateau-Thierry, P., Laxon, S. W., Mallow, U., Mavrocordatos, C., Phalippou, L., Ratier, G., Rey, L., Rostan, F., Viau, P. and Wallis, D. W.: CryoSat: A mission to determine the fluctuations in Earth's land and marine ice fields, Adv. Sp. Res., 37(4), 841–871, doi:10.1016/j.asr.2005.07.027, 2006a.

Wingham, D. J., Shepherd, a, Muir, a and Marshall, G. J.: Mass balance of the Antarctic ice sheet., Philos. Trans. A. Math. Phys. Eng. Sci., 364(1844), 1627–35, doi:10.1098/rsta.2006.1792, 2006b.

Wouters, B., Martin-Espanol, A., Helm, V., Flament, T., van Wessem, J. M., Ligtenberg, S. R. M., van den Broeke, M. R. and Bamber, J. L.: Dynamic thinning of glaciers on the Southern Antarctic Peninsula, Science (80-.)., 348(6237), 899–903, doi:10.1126/science.aaa5727, 2015.

Zwally, H. J., Bindschadler, R. a, Brenner, a C., Major, J. a and Marsh, J. G.: Growth of greenland ice sheet: measurement., Science, 246(4937), 1587–1589, doi:10.1126/science.246.4937.1587, 1989.

Zwally, H. J., Giovinetto, M. B., Li, J., Cornejo, H. G. and Beckley, M. a: Mass changes of the Greenland and Antarctica ice sheets and shelves and contributions to sea level rise: 1992-2002, J. Glaciol., 51(175), 509, doi:10.3189/172756505781829007, 2005.

Zwally, H. J., Jun, L., Brenner, A. C., Beckley, M., Cornejo, H. G., Dimarzio, J., Giovinetto, M.

1147 B., Neumann, T. a, Robbins, J., Saba, J. L., Donghui, Y. and Wang, W.: Greenland ice sheet
1148 mass balance: distribution of increased mass loss with climate warming; 2003–07 versus 1992–
1149 2002, J. Glaciol., 57(201), 88–102, doi:10.3189/002214311795306682, 2011.
1150 Zwally, H. Jay, Mario B. Giovinetto, Matthew A. Beckley, and Jack L. Saba: Antarctic and
1151 Greenland drainage systems, GSFC Cryospheric Sciences Laboratory, at
1152 http://icesat4.gsfc.nasa.gov/cryo_data/ant_grn_drainage_systems.php, 2012

Tables:

Table 1: Accuracy (Mean), precision (SD) and the total RMS-error (RMSE) of surface elevation from CryoSat-2 observations compared to IceBridge ATM elevations. Here, the LRM mode represents the interior of the ice sheet and SIN the marginal high relief areas.

JPL	**Mean (m)**	**SD (m)**	**RMSE (m)**
LRM	0.00	0.43	0.45
SIN	-0.52	0.58	0.82
ESA	**Mean (m)**	**SD (m)**	**RMSE (m)**
LRM	-1.06	0.89	1.40
SIN	-0.90	1.05	1.13

Johan Nilsson 9/22/2016 3:42 PM
Deleted: ,

Johan Nilsson 9/22/2016 3:42 PM
Deleted: *and the residual slope error (SE)*

Johan Nilsson 9/22/2016 3:42 PM
Formatted Table

Table 2: Accuracy (Mean), precision (SD) and the total RMS-error (RMSE) of surface elevation changes from CryoSat-2 derived from two independent methods [Surface Fit (SF) an the Crossover (XO) method], compared to IceBridge ATM data.

JPL - LRM	**Mean (m)**	**SD (m)**	**RMSE (m)**
SF	0.11	0.67	0.70
XO	0.24	0.72	0.78
ESA - LRM	**Mean (m)**	**SD (m)**	**RMSE (m)**
SF	0.25	1.51	1.57
XO	0.60	1.02	1.20
JPL - SIN	**Mean (m)**	**SD (m)**	**RMSE (m)**
SF	0.30	0.58	0.66
XO	-0.60	1.26	1.26
ESA - SIN	**Mean (m)**	**SD (m)**	**RMSE (m)**
SF	0.34	1.06	1.11
XO	-0.21	1.44	1.44

Johan Nilsson 9/23/2016 3:39 PM
Deleted: ,

Johan Nilsson 9/23/2016 3:39 PM
Deleted: *and the residual slope error (SE)*

Johan Nilsson 9/20/2016 10:22 AM
Deleted: *three*

Johan Nilsson 9/20/2016 10:22 AM
Deleted: ,

Johan Nilsson 9/20/2016 10:22 AM
Deleted: *and the DEM method (DM)*

Johan Nilsson 9/22/2016 3:42 PM
Formatted Table

Johan Nilsson 9/20/2016 10:21 AM
Deleted: DM ... [6]

Johan Nilsson 9/20/2016 10:21 AM
Deleted: DM ... [7]

Johan Nilsson 9/20/2016 10:21 AM
Deleted: DM ... [8]

Johan Nilsson 9/20/2016 10:21 AM
Deleted: DM ... [9]

Table 3: Validation of four different DEMs, compared to IceBridge ATM elevation data. Based on the weighted (number of samples) average of the four different ATM campaigns from 2011 to 2014. Elevation values at each ATM location were estimated by bilinear interpolation for each DEM product.

DEM	Mean (m)	SD (m)	RMSE (m)
AWI	-1.35	5.95	6.12
GIMP	-1.13	7.22	7.32
JPL	-0.87	6.31	6.39
ESA	-2.83	6.13	6.76

Table 4: Individual basin volume changes (km^3a^{-1}) for the Surface-Fit (SF) and Crossover (XO) method for the JPL and ESA product for the time period Jan-2011 to Jan-2015, with corresponding volumetric error.

Basin	SF – JPL	XO – JPL	SF - ESA	XO - ESA
1	-26 ± 8	-23 ± 12	-9 ± 14	-11 ± 15
2	5 ± 8	0 ± 13	31 ± 16	30 ±16
3	-38 ± 9	-34 ± 19	-46 ± 16	-31 ± 23
4	-36 ± 7	-37 ± 15	-42 ± 12	-16 ± 18
5	-19 ± 4	-27 ± 11	-19 ± 7	-6 ± 13
6	-72 ± 7	-71 ± 12	-75 ± 13	-79 ± 18
7	-56 ± 7	-51 ± 10	-41 ± 14	-35 ± 15
8	-48 ± 8	-45 ± 12	-23 ± 15	-27 ± 17
TOT	**-289 ± 20**	**-288 ± 37**	**-224± 38**	**-174 ± 48**

Deleted: ,…Crossover (XO) and DEM (D… [10]
Johan Nilsson 9/20/2016 10:23 AM
Formatted Table … [11]
Johan Nilsson 9/22/2016 11:38 AM
Deleted: 6
Johan Nilsson 9/22/2016 11:43 AM
Deleted: 9
Johan Nilsson 9/22/2016 11:39 AM
Deleted: 12
Johan Nilsson 9/22/2016 11:45 AM
Deleted: 2
Johan Nilsson 9/22/2016 11:38 AM
Deleted: 7
Johan Nilsson 9/22/2016 11:43 AM
Deleted: 10
Johan Nilsson 9/22/2016 11:39 AM
Deleted: 14
Johan Nilsson 9/22/2016 11:45 AM
Deleted: 3
Johan Nilsson 9/22/2016 11:38 AM
Deleted: 6
Johan Nilsson 9/22/2016 11:43 AM
Deleted: 15
Johan Nilsson 9/22/2016 11:39 AM
Deleted: 13
Johan Nilsson 9/22/2016 11:45 AM
Deleted: 0
Johan Nilsson 9/22/2016 11:38 AM
Deleted: 4
Johan Nilsson 9/22/2016 11:43 AM
Deleted: 1
Johan Nilsson 9/22/2016 11:39 AM
Deleted: 9
Johan Nilsson 9/22/2016 11:45 AM
Deleted: 4
Johan Nilsson 9/22/2016 11:38 AM
Deleted: 2
Johan Nilsson 9/22/2016 11:43 AM
Deleted: 8
Johan Nilsson 9/22/2016 11:39 AM
Deleted: 4
Johan Nilsson 9/22/2016 11:45 AM
Deleted: 9
Johan Nilsson 9/22/2016 11:39 AM
Deleted: 6
Johan Nilsson 9/22/2016 11:43 AM
Deleted: 0
Johan Nilsson 9/22/2016 11:39 AM
Deleted: 1
Johan Nilsson 9/22/2016 11:46 AM
Deleted: 8
Johan Nilsson 9/22/2016 11:39 AM
Deleted: 6
Johan Nilsson 9/22/2016 11:39 AM
Deleted: 2
Johan Nilsson 9/22/2016 11:46 AM
Deleted: 4
Johan Nilsson 9/22/2016 11:39 AM
Deleted: 6
Johan Nilsson 9/22/2016 11:43 AM
Deleted: 0
Johan Nilsson 9/22/2016 11:39 AM
Johan Nilsson 9/22/2016 11:46 AM
Johan Nilsson 9/22/2016 11:40 AM
Johan Nilsson 9/22/2016 11:44 AM
Johan Nilsson 9/22/2016 11:40 AM
Johan Nilsson 9/22/2016 11:48 AM

Figures:

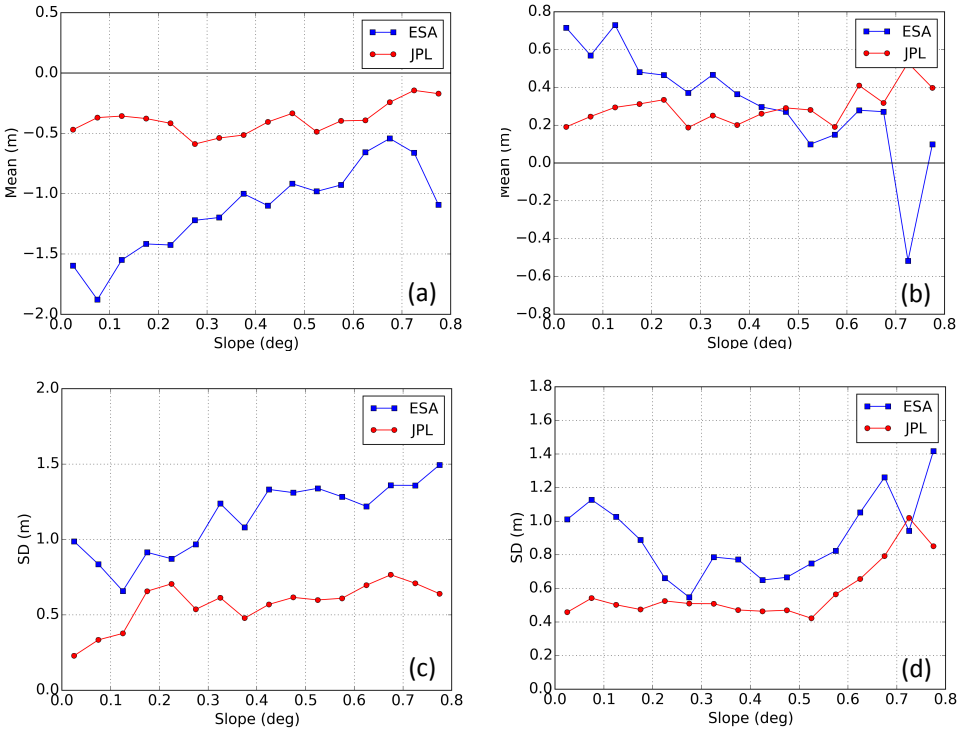

Figure 1: Validation of surface elevations (2012) (a,c) and surface elevation changes (2011-2014) (b,d) compared to IceBridge ATM, as a function of surface slope. The accuracy of the measurement is defined as the mean-value (Mean) of the CryoSat-2-ATM residuals and the precision as the standard deviation (SD).

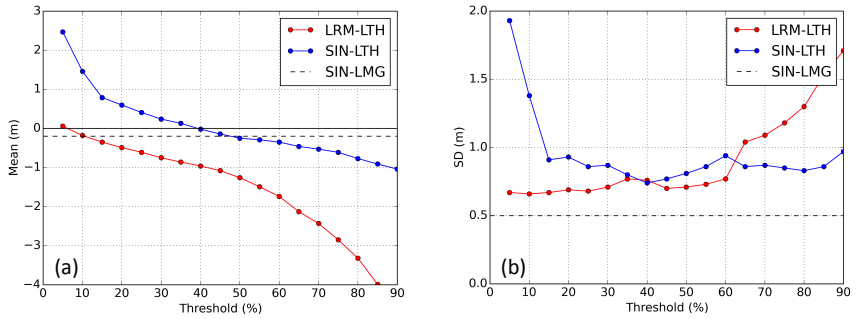

Unknown
Formatted: Font:Bold, Font color: White

Figure 2: Accuracy (a) and precision (b) of JPL surface elevations, relative to near-coincident ATM elevations, estimated from a Leading-edge Threshold retracker (LTH, dots) over Jakobshavn and NE-Greenland and the Leading-edge Maximum Gradient (LMG retracker, (dashed grey line) for the SIN-mode. The accuracy is defined as the mean-value (Mean) of the CryoSat-2-ATM residuals and the precision as the standard deviation (SD).

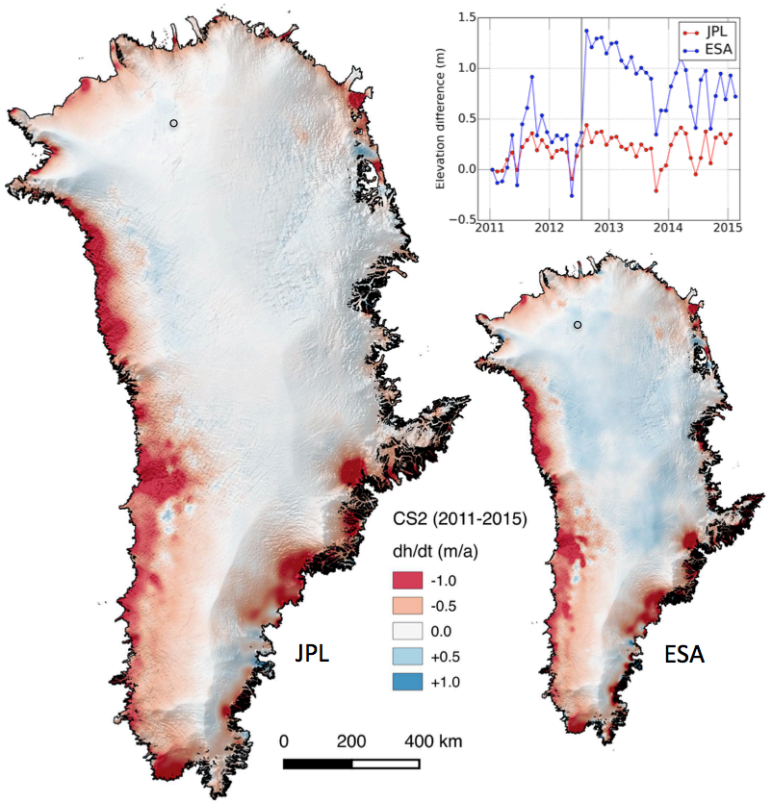

Figure 3: 2011-2015 elevation changes estimated from the surface-fit methods for the estimated L2 products. The time series depicted in the figure has been extracted from the NEEM camp (77°27'N 51°3.6'W), indicated by the black circle. The time series show clearly the effect of the 2012 melt event, indicated by the grey vertical line, on the retrieved surface elevations. The JPL product produced a total volume change of -289 ± 20 km^3 a^{-1} while the estimated total volume change of the ESA product totaled -224 ± 38 km^3 a^{-1}. This corresponds to -29 versus 38 km^3 a^{-1} (H > 2000 m) and -259 versus -262 km^3 a^{-1} (H < 2000 m) for the JPL and ESA product respectively. Images have been smoothed with a 10 km median filter for visualization purposes. The 1x1 km ice sheets mask used in this figure was constructed from polygons obtained from Frank Paul at the University of Zurich (personal communication).

Johan Nilsson 9/23/2016 3:23 PM
Deleted: 2

Johan Nilsson 9/22/2016 11:37 AM
Deleted: 16

Johan Nilsson 9/22/2016 11:37 AM
Deleted: 1

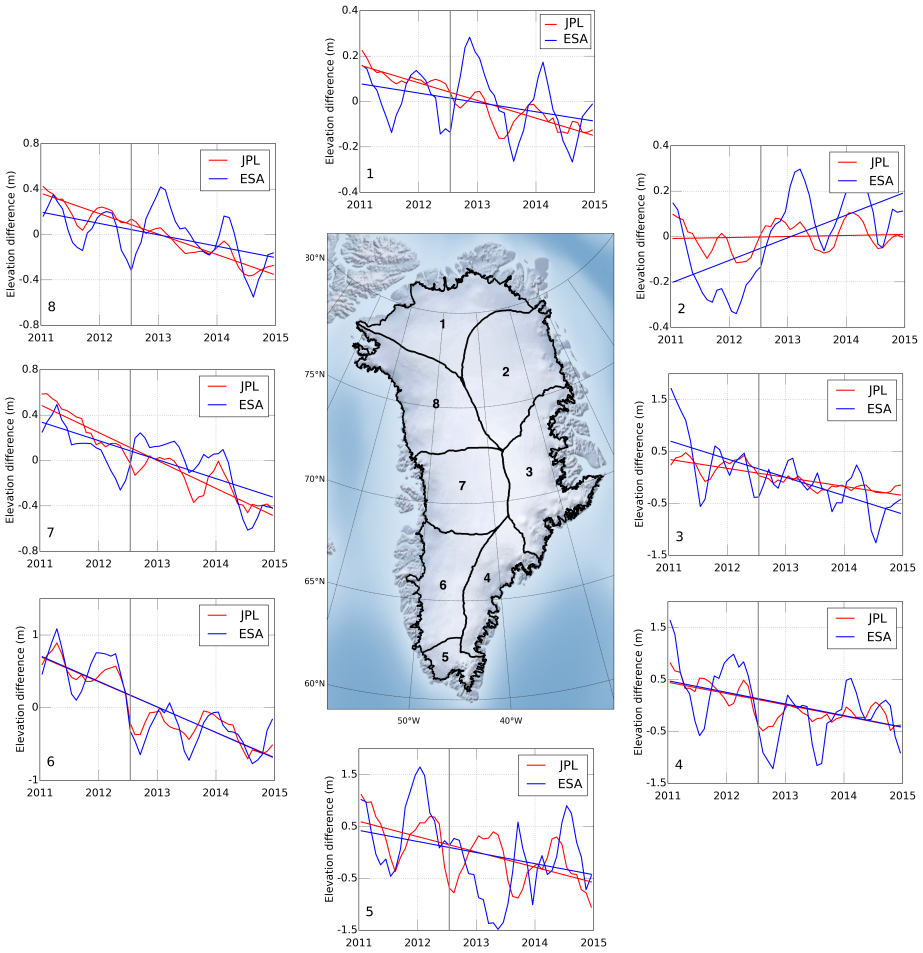

Figure 4. Monthly elevation change time-series for 8 large drainage basins of the Greenland Ice Sheet. Time-series have been smoothed using a 3-month moving average for improved visualization. The grey vertical line indicates the timing of the 2012 melt event.

Johan Nilsson 9/23/2016 3:24 PM
Deleted: *3*

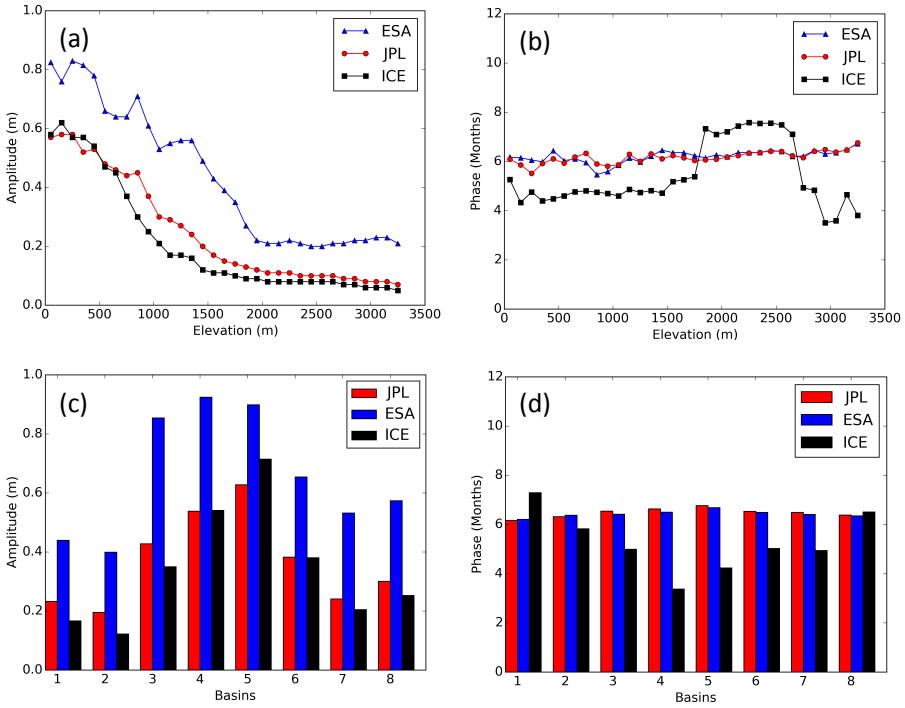

Figure 5: Estimated seasonal amplitude (a,c) and phase of the maximum amplitude (b,d) from the surface-fit method for CryoSat-2 [ESA (blue) and JPL (red)] compared to ICESat (ICE, black)). Values are compared using a search radius of 500 m, using the closest point within this distance, and the phase offset is referenced from 1st of January. The values of amplitude and phase are then binned according to elevation using the median value within 100 m intervals.

Johan Nilsson 9/20/2016 11:00 AM
Deleted: *5*

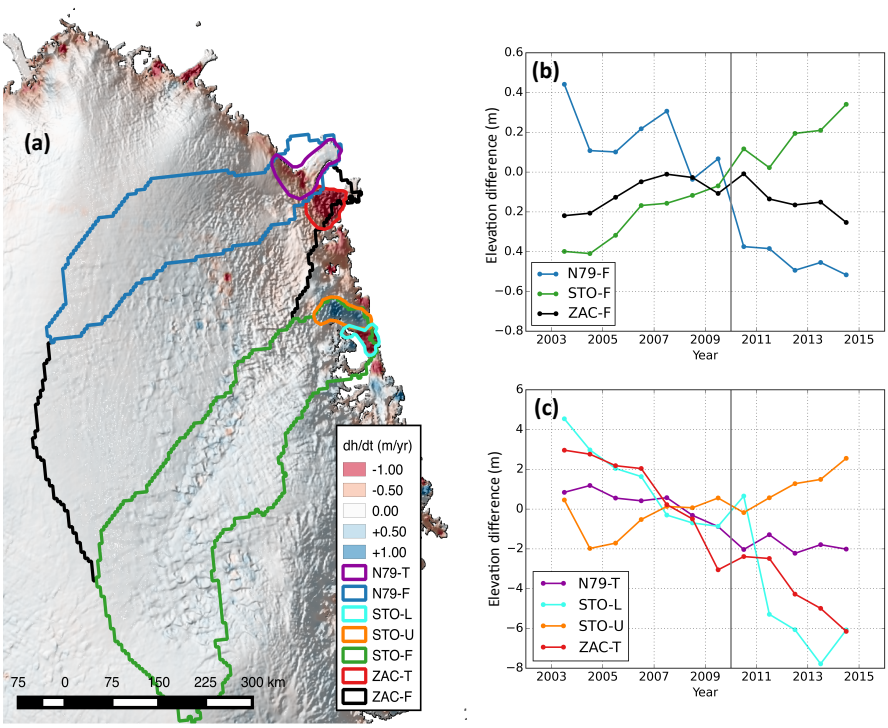

Figure 6: Northeast part of the Greenland Ice Sheet showing surface elevation change (a) from CryoSat-2 JPL-solution (2011-2015), with corresponding hydrological basin outlines. The hydrological basins are separated into full basins size (b) and to the terminus areas (c). Sub-figures (b) and (c) shows a merged 12 year annual elevation time series from ICESat and CryoSat-2 for each color-coded area in (a). The derived elevation time series was formed using the surface-fit method described in Section (3.1). The elevation change map is overlaid onto the CryoSat-2 hill shaded DEM based on surface heights from Jul-2010 to Feb-2015.

Johan Nilsson 9/20/2016 11:00 AM
Deleted: *6*

Response to reviewer #1 (L. Schröder)

We would first like to thank the reviewer for his constructive and insightful comments, which has greatly helped to improve this manuscript.

The reviewer's remarks are in bold font, while the author's response is in italic form below.

General Comments:

The reviewer has in his analysis of the paper asked for more substantial proof of the sensitivity of the two retrackers used in this study (threshold versus functional-fit) to changes in snow-pack properties. To address this we have merged Figure (2 & 4) and expanded it to include a local time-series for the NEEM camp, which encompasses the time of the melt event. This figure clearly shows the effect of the change in snow-pack conditions at time of the 2012 melt event, and the subsequent introduction of a clear elevation bias in this case the ESA retracker, with a magnitude of ~1 m, which can be seen in Figure-2

In the case of the residual slope bias/error we have chosen to remove this metric. This was done to make the elevation and elevation change comparison more coherent. In the case of the elevation a clear linear relation, depended on topography and snow physics, can be found (penetration bias and precision in the retrieval of measurements) and easily quantified using a linear model. However, this does not hold for the elevation changes where the bias is mostly related to climatological effects, which may change over time, and further the slope-error is not easily characterized by a linear trend (or higher polynomials). This due to the 2012 melt event effect on the standard deviation in low sloping areas (0-0.3°) for the ESA product. So, we have chosen to remove this metric and guide the reader to Figure-1, where these different effects can clearly be seen and judged visually.

l.12: Expr: This when compared

Changed the statement by merging it with the previous sentence.

l.41: add brackets around "(e.g. Gardner et al., 2013; Shepherd et al., 2012)"

Brackets where added around the citation.

l.44: Expr: “the characteristics of which is”

Removed the expression from the sentence

l.60: Expr: “methods from improving”

The sentence was changed where “from” was replaced by “for”.

l.77: I think 1° is no “low sloping terrain” anymore for radar altimetry. The switch to SARIn happens already at lower slopes (~0.5°).

[A] The reviewer has a good point and we have therefore removed the numbers to make the statement more generic.

l.101: In Baseline-B LRM has only 128 bins so I think the interval should end some bins before.

Perfectly true! This statement belongs to the SIN retracker and was unfortunately overlooked. For the LRM-mode only peak indexes larger than 20 are used in the retracking procedure.

l.126: don’t use the surname in the citation

This has been removed accordingly.

l.128: SIN mode allows... repeats more or less the last sentence

The sentence was re-written to remove any repetitive nature.

l.142ff: This is not totally clear to me. Please explain a bit more in detail what the “coherence range power image” is.

*This was changed to “Coherence as a function of range”, e.g. across track coherence (an array of size Nobs*512) for each measurement in the track*.

l.205ff: Please use different letters for different variables (not again a0,a1).

This has also been pointed out by reviewer #2 and has been change accordingly in the entire manuscript.

l.323: I guess no ICESat campaign biases have been applied as in Nilsson et al., 2015b. Maybe the influence of those biases (~10 cm) on the seasonal amplitude and phase is not too big, but anyways this should be mentioned and discussed when taking ICESat as a reference for the "true surface amplitude" (l.551)

This is a good point and we have added a paragraph detailing this in the ICESat section. Further, a statement was also added in line 577 detailing that the correction has not been applied.

l.407: Why has no attempt been made? Please explain!

Quantifying the accuracy of the different DEM's is inherently difficult, as they are based on both different types of datasets and acquired over different time spans, many not entirely consistent with the temporal coverage of the ATM data. For this case the interest was to compare them in a relative fashion to judge their quality. It's of course expected that older DEM's would show a larger statistical difference from the ATM data used in the comparison. However, as stated in the manuscript, we do not attempt to provide a full validation framework of the different DEM's, only a relative comparison.

l.425: repetition: processing steps

Has been removed to improve reading

l.692: remove "by"

Removed

In Tab.2 as it summarizes results of elevation change I guess the units shall be m*aˆ-1.

The units on the table are correct, as we have chosen to multiply it with the time-span of each elevation change data set. This was done to make the statistics/errors more comparable between time periods, as the error is expected to decrease with time.

Response to reviewer #2 (Anonymous)

Firstly we would like to thank the reviewer for taking the time to review our manuscript. We are thankful for the insightful and constructive comments that have been provided, which we feel will improve our manuscript.

The reviewer's remarks are in bold font, while the author's response is in italic form below.

General remarks:

(1) *In response to the rational of using different elevation change methods we have included a sentence in the introduction describing the choice of different methods. Further, we have also chosen to remove the DEM-method from the manuscript, as we feel that this method does not bring any new insight to the study and can be reproduced by the SF-method (as seen with the ICESat/CryoSat time series). We hope that this will make the manuscript more concise.*

(2) *To produce a manuscript of reasonable length we chose to keep the general description of the processing chain generic and highlight the details that make the processing scheme unique but agree that more details on the retracker in the main document would be beneficial. We have therefore moved the retracker comparison from the SI to the validation section of the main manuscript. For the curious or more technical reader we have supplied reference that provides a more technical description of the algorithms used.*

(3) *We agree with the reviewer that the notations in the different equations have to be improved. This has been changed accordingly through out the manuscript. Please see track changes version of the revised manuscript.*

Detailed remarks:

Describing the error of the volume change estimations (lines 436-446) the authors treat the errors as systematic errors rather than random errors and thus overestimate the volume change errors.

We have changed Equation 12 to correct for this and we are grateful that this was pointed out to us. All volume change errors have been updated to encompass the corrected error propagation.

The error of the elevation change (lines 447-459) describes the error of the mean elevation change of the entire ice sheet rather than the error of a

single elevation change estimate. This error is not referred in the manuscript.

The single-observation uncertainty, or σ_{obs}, is estimated from the CryoSat-2 – ATM residuals as the RMSE. The derivation of this error source is described in the "Error Budget" section on line 583. We have rewritten this section to make it clearer how the single observation error and interpolation errors are defined.

Lines 327-333: what ATM products were used for the study and from where were those obtained? NSIDC distributes both individual ATM footprint locations and average ice sheet elevations for larger regions (ICESS). Ice sheet elevation accuracies are 0.071-0.085 m according to Krabill et al., 2002 – more like 0.1 m than cm level as quoted in the manuscript.

The ATM data obtain from the NSIDC was the ILATM2 product (IceBridge ATM L2 Icessn Elevation, Slope, and Roughness, Version 2), which contains the measured surface elevation, slope and roughness for each measurement averaged to 80 resolution with 40 m spacing. We have changed the manuscript to reflect this, where we have put in the source of the data and the accuracies.

Lines 463-491: this section provides a verbal description of tables. Adding the percentage of improvement would be more informative.

If we understand correctly the reviewer asks for the percentage after each numbered value? This, as far as we believe, has been met, as the percentage values for RMSE is stated in the manuscript, which encompasses both the mean and standard deviation.

Lines 573-583 and later: please use the accepted names of these glaciers: Zachariæ Isstrøm, Nioghalvfjerdsfjorden and Storstrømmen glaciers.

This has been changed accordingly.

Lines 686-697: this seems to be a missed opportunity to emphasize the good spatial and temporal resolution of CryoSat-2 observations. The recovering surge of Storstrømmen glacier has been well documented, and additional references would improve the manuscript.

The reviewer has a good point here and we have added additional references documenting the recovery at Storstrømmen. We thank the reviewer for suggesting this improvement.

Table 2. Please include the period the elevation changes refer to Figure 2. What ice sheet mask was used to define the boundary of the ice sheet?

Figure 3. Were the monthly changes determined by the DEM method?
Figure 4. There is no reference to this figure in the text. Can this figure be merged with Figure 2? Does not seem to include additional information.
Figure 5. I assume that all the values here are average/mean values. If yes, this should be stated in the caption

We have added the periods to the figures showing time period of elevation change. The ice sheet mask was provided by personal communication with Frank Paul at University of Zurich. This has also been added to the manuscript.

In the case of the monthly time-series they where generated using the DEM-method. However, as the DEM-method has been removed these have been replaced by the time-series from the surface-fit method.

Figure-2 and 4 has now been merged into one main figure to reduce the number of figures overall.

Figure-5 contains the median-values inside each 100 m elevation interval using. This has been added to the caption to make it clear